JOURNAL OF GEOPHYSICAL RESEARCH: SOLID EARTH, VOL. 118, 1277–1303, doi:10.1002/jgrb.50121, 2013

Permanent upper plate deformation in western Myanmar during the great 1762 earthquake: Implications for neotectonic behavior of the northern Sunda megathrust

Yu Wang,[1,2] J. Bruce H. Shyu,[3] Kerry Sieh,[2] Hong-Wei Chiang,[2,3] Chung-Che Wang,[3] Thura Aung,[4] Yu-nung Nina Lin,[1] Chuan-Chou Shen,[3] Soe Min,[4] Oo Than,[5] Kyaw Kyaw Lin,[5] and Soe Thura Tun[4]

Received 29 November 2012; revised 4 February 2013; accepted 5 February 2013; published 28 March 2013.

[1] The 1762 Arakan earthquake resulted from rupture of the northern Sunda megathrust and is one of those rare preinstrumental earthquakes for which early historical accounts document ground deformations. In order to obtain more comprehensive and detailed measurements of coseismic uplift, we conducted comprehensive field investigations and geochronological analyses of marine terraces on the two largest islands in western Myanmar. We confirm 3–4 m of coseismic coastal emergence along southwestern Cheduba Island, diminishing northeastward to less than 1 m. Farther northeast, uplift associated with the earthquake ranges from slightly more than 1 m to 5–6 m along the western coast of Ramree Island but is insignificant along the island's eastern coast. This double-hump pattern of uplift coincides with the long-term anticlinal growth of these two islands. Thus, we propose that the 1762 earthquake resulted from slip on splay faults under the islands, in addition to rupture of the megathrust. Elastic modeling implies that fault slip during the 1762 earthquake ranges from about 9 to 16 m beneath the islands and corresponds to a magnitude of M_w 8.5 if the rupture length of the megathrust is ~500 km. The island's uplift histories suggest recurrence intervals of such events of about 500–700 years. Additional detailed paleoseismological studies would add significant additional detail to the history of large earthquakes in this region.

Citation: Wang, Y., et al. (2013), Permanent upper plate deformation in western Myanmar during the great 1762 earthquake: Implications for neotectonic behavior of the northern Sunda megathrust, *J. Geophys. Res. Solid Earth*, *118*, 1277–1303, doi:10.1002/jgrb.50121.

1. Introduction

[2] Coseismic deformation above subduction megathrusts is a key to understanding great earthquake ruptures along convergent plate margins. Usually, deformation patterns imply rupture solely on the underlying megathrust, as in the 2005 Nias and 2007 Solomon Islands earthquakes [e.g., *Briggs et al.*, 2006; *Konca et al.*, 2007; *Taylor et al.*, 2008]. Less commonly, upper plate structures are also involved, as in the cases of the great 1964 Alaskan and 1946 Nankaido earthquakes [e.g., *Plafker*, 1965; *Fukao*, 1979; *Kato*, 1983; *Park et al.*, 2000]. Although they are smaller than their associated megathrusts, upper plate structures may play significant roles in the generation of seismic shaking or tsunami, as appears to have been the case with the great 2004 Sumatran earthquake and tsunami [*DeDontney and Rice*, 2012]. Structures in the fore-arc region may be also related to major asperities of large megathrust earthquakes [e.g., *Sugiyama*, 1994; *Wells et al.*, 2003]. Nineteenth century reports of coastal uplift during the great 1762 Arakan earthquake in western Myanmar are intriguing in this regard, because they imply that upper plate structures played a role in the earthquake.

[3] At about the same time that *Darwin* [1845] was documenting and publishing his famous observations of deformation associated with the great 1835 Chilean earthquake, British naval officers documented coastal emergence that may have occurred during the 1762 Arakan earthquake. Their observations suggested up to 7 m of coseismic uplift on Cheduba (Man-Aung) and neighboring Ramree Islands [*Halsted*, 1841; *Mallet*, 1878] (Figure 1). They also described associated flights of marine terraces. These

[1]Division of Geological and Planetary Sciences, California Institute of Technology, Pasadena, California, USA.
[2]Earth Observatory of Singapore, Nanyang Technological University, Singapore.
[3]Department of Geosciences, National Taiwan University, Taipei, Taiwan.
[4]Myanmar Earthquake Committee, Myanmar Engineering Society, Yangon, Myanmar.
[5]Department of Meteorology and Hydrology, Yangon, Myanmar.

Corresponding author: J. Bruce H. Shyu, Department of Geosciences, National Taiwan University, Taipei 10617, Taiwan. (jbhs@ntu.edu.tw)

2169-9313/13/10.1002/jgrb.50121

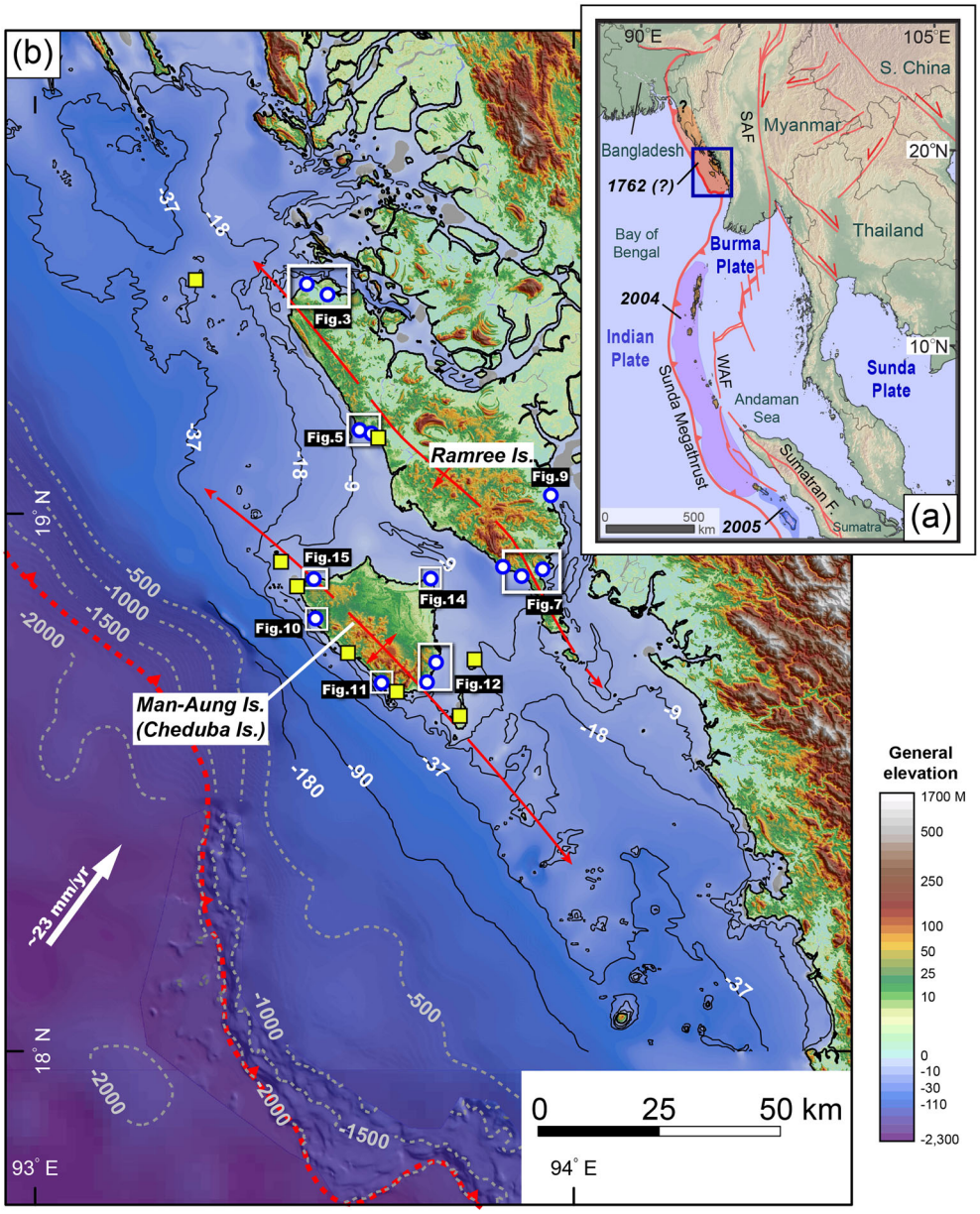

Figure 1. Cheduba (Man-Aung) and Ramree Islands are the expressions of two active antiforms above the Sunda megathrust offshore the western coast of Myanmar. (a) The last seismic ruptures of the northern Sunda megathrust, between the Indian and the Burma plates. Orange color depicts the inferred 1762 Arakan rupture from historical reports. This ~500 km long seismic patch is the only megathrust-related rupture north of the 2004 patch (shown in purple, after *Chlieh et al.* [2007]) from the 18th century to present. Red lines are major active faults in Southeast Asia (after *Le Dain et al.* [1984]), where most of the major faults are strike-slip faults on the Burma and the Sunda plates. Blue box shows the area of Figure 1b. SAF: Sagaing fault system; WAF: West Andaman fault. (b) The accretion-related topography above the Sunda megathrust and our survey locations in Cheduba and Ramree Islands. This section of the megathrust receives ~23 mm/yr of oblique plate convergence from the northeastward motion of the Indian plate [*Socquet et al.*, 2006]. This plate convergence creates a series of megathrust-parallel underwater ridges within the accretionary prism. Cheduba and Ramree Islands are the two highest portions of these tectonic ridges. Black solid contours are modified from the U.S. Army topography maps [*U.S. Army Map Service*, 1955a, 1955b]. Grey dashed contours are from ETOPO-1 [*Amante et al.*, 2009]. The high-resolution bathymetry along the trench front is digitized from *Nielsen et al.* [2004]. Yellow squares indicate the observation points in the 19th century [*Halsted*, 1841; *Mallet*, 1878]. White dots represent the survey locations of this study, between 2010 and 2011.

observations led them to speculate that these coastlines were being permanently uplifted during similar successive earthquakes [*Halsted*, 1841]. The permanence of uplift implied by the flights of terraces does indeed suggest repeated inelastic deformation within the accretionary prism.

[4] Though intriguing, the 19th century observations are too sparse to enable one to conclude much about the nature of the faulting that caused the deformations or about the magnitude of the earthquake. One limitation is that most of the observations were made decades after the earthquake, so assignment of the observed deformations solely to the 1762 event is dubious. Another limitation of the historical observations is their small geographic spread. Most of the reliable observations are along the western side of Cheduba (Man-Aung) Island (Figure 1b), with just a few other accounts from the west coast of Myanmar and Bangladesh.

[5] This irregular and sparse distribution of observations and the uncertainty of the timing of uplift are inadequate for construction of a useful deformation pattern for the 1762 earthquake. Thus, we decided to reevaluate the 19th century observations and to improve the quantity and quality of observations via a field investigation that included new geomorphic measurements and precise geochronological analyses of uplifted coastal features.

[6] In the pages that follow, we describe our observations of the vertical deformation along the coasts of Ramree and Cheduba Islands associated with the 1762 event via measuring several different sea level markers. U-Th dating techniques [*Shen et al*., 2003, 2012] on a multicollector inductively coupled plasma mass spectrometer (MC-ICP-MS), Thermo Fisher Neptune, at the High-Precision Mass Spectrometry and Environment Change Laboratory (HISPEC), National Taiwan University, were used to determine the time of uplift of these features. Ages of several carbonate samples were also determined by radiocarbon dating technique. Moreover, we describe our mapping of regional geomorphic features, which provides the neotectonic context for understanding the dated uplifted features. We then discuss the possible sources and seismic parameters of the 1762 Arakan earthquake, including its earthquake magnitude and the recurrence interval.

2. Active Tectonic Context

[7] The northern Sunda megathrust is the nominal boundary between the Indian and the Burma plates. In reality the boundary is not so simple, because thick sediments of the Bengal Fan sit atop the downgoing Indian Ocean lithosphere, and much of this sedimentary section is being folded rather than subducted [*Curray*, 1991; *Curray et al*., 2003]. These sediments sit at the boundary of two plates that are converging obliquely at about 23 mm/yr [*Socquet et al*., 2006] (Figure 1b). Most of this dextral-oblique convergence appears to be taken up by the megathrust and structures above it in the accretionary prism.

[8] In the vicinity of Cheduba and Ramree Islands, the Bengal Fan sediments are 8–12 km thick and exhibit a wide zone of folding and shortening above the downgoing Indian Ocean lithosphere. Two active trench-parallel antiforms are readily apparent in the bathymetry and topography. Cheduba Island, 40–60 km northeast of the deformation front, is the subaerial expression of the western of these two; and Ramree Island, 70–100 km away from the trench, is the manifestation of the other (Figure 1b). Both antiforms are doubly plunging and are asymmetric, as evidenced by their southwestern flanks being clearly steeper than their northeastern flanks. In each case, cumulative uplift appears to have been greater near their southwestern flanks, since their highest topography is closer to their southwestern flanks. Several studies have discussed the nature of these upper plate structures. For example, *Nielsen et al*. [2004] documented the active folds and faults within the accretionary prism near the deformation front. *Maurin and Rangin* [2009] suggested that a northeast dipping blind thrust fault 20 km west of Cheduba Island initiated after the late Pliocene. Although there are no constraints on the rates of deformation, the existence of the antiforms strongly implies that a significant amount of Indian-Burma plate convergence is occurring within the accretionary wedge. Thus, the upper plate structures are potential seismic sources in this area.

[9] In this context, it is not surprising that abundant evidence for geologically recent uplift exists on and in the vicinity of Cheduba and Ramree Islands. Flights of marine terraces have long been known along western Myanmar coast. *Brunnschweiler* [1966] reported post-Pliocene marine terraces about 45–60 m above sea level along western Cheduba Island and 30 m high terraces along western Ramree Island. *Than Tin Aung et al*. [2008] described a series of marine terraces north of Ramree Island, the oldest of which is about ~3000 years old and 6–16 m above current mean sea level (MSL).

[10] Several earlier observers suggested that the uplift occurred during seismic events: *Halsted* [1841] observed that the elevation difference between each marine terrace on western Cheduba Island is identical to the amount of the latest uplift there. *Mallet*'s [1878] observations suggested to him that no changes occurred between Captain Halsted's observations and his own visit in the late 19th century. More recently, *Shishikura et al*. [2009] supported this view; they suggested that the elevation of the lowest terrace on western Cheduba Island is similar to the elevation recorded by Captain Halsted. This implies that no appreciable net vertical movement has occurred since the mid-19th century. Taken together, these observations imply that the majority of uplift occurs during or right after earthquakes and that recovery during the interseismic period is minimal. This deformation behavior thus provides us an excellent opportunity for studying the plausible coseismic coastal uplift that occurred 250 years ago.

3. Sea Level Indicators

[11] To constrain land-level changes along the coasts of the islands precisely, one must measure the elevations of uplifted sea level indicators relative to their modern equivalents. These indicators may be either marine organisms preserved in their living position or erosional and depositional features. Sea level indicators form at a range of locations between high- and low-water spring tides; therefore, on a mesotidal coast as in western Myanmar, where mean tidal range is >2 m, these indicators form over a vertical range of about 3 m, as shown in Figure 2.

[12] The major types of sea level indicators that we used comprise coastal erosional features (shoreline angles, sea

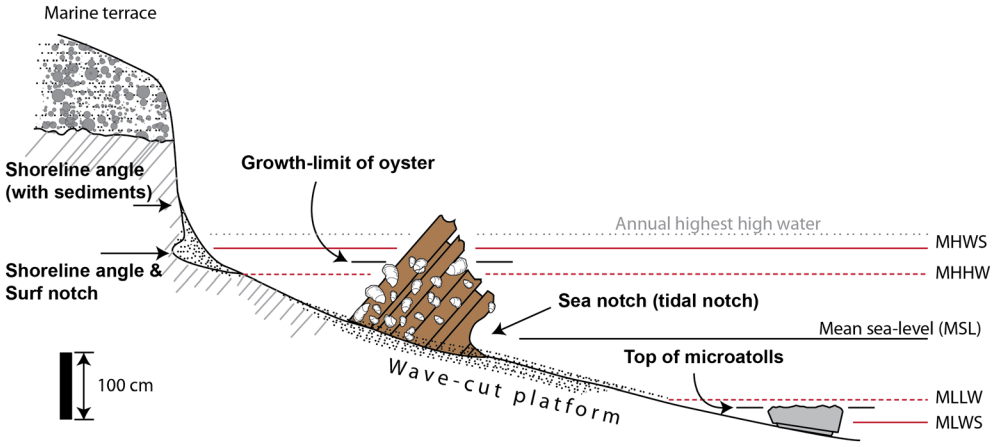

Figure 2. Natural sea level indicators and their relationships with the tidal levels in the area of Cheduba and Ramree Islands. This schematic diagram shows the modern positions of various sea level indicators in mesotidal environments (with tidal range of 2–4 m). The upper growth limit of oysters and the coastal erosional features (shoreline angles and wave-cut notches) are mostly related to the water level from mean sea level (MSL) to high tide. The top of coral microatolls, however, represents the water level that is ~1–2 m lower than the other features. The elevation of microatolls is inferred from *Kayanne et al*. [2007], and the other indicator's elevations are from this study. MHWS: mean high-water springs; MHHW: mean higher high water; MLLW: mean lower low water; MLWS: mean low-water springs.

notches and wave-cut platforms) and the living position of marine organisms (coral microatolls and oysters). Each of these has been extensively used elsewhere around the world to measure sea level histories in a range of tidal environments [e.g., *Chappell et al*., 1983; *Hull*, 1987; *ten Brink et al*., 2006; *Meltzner et al*., 2010].

[13] To estimate the relationship between the sea level indicators and their associated water levels, we first measure the modern indicators' elevations with respect to the water level at the time of survey. We then relate this measured elevation to present MSL, using tidal predictions from the software package NLOADF (SPOTL v.3.2.4) [*Agnew*, 1997] and the regional harmonic tidal solutions for the Bay of Bengal from the Oregon State University [http://volkov.oce.orst.edu/tides/BBay.html]. This method is reliable for estimation of water level in western Sumatra [e.g., *Briggs et al*., 2006; *Meltzner et al*., 2006, 2010].

[14] Our survey results and other studies imply that most of the indicators we used reliably constrain paleo–water levels with precisions ranging from about ±0.25 m to about ±1 m [e.g., *Chappell et al*., 1983; *ten Brink et al*., 2006; *Lewis et al*., 2008]. This is a considerable improvement in precision from just correlating the average terrace elevation to current MSL, which may have more than 2 m of uncertainty in this mesotidal environment.

[15] Below, we describe the five major sea level indicators that we use and their relationship to the tidal datum.

3.1. Biological Indicators

3.1.1. Oysters

[16] Emerged oysters have been widely used to constrain land-level changes [e.g., *Davis et al*., 2000; *Awata et al*., 2008; *Lewis et al*., 2008; *Hsieh et al*., 2009]. Their upper growth limit is usually restricted below high-water level [e.g., *Kelletat*, 1988; *Beaman et al*., 1994; *Lewis et al*., 2008; *Hsieh et al*., 2009]. On Ramree and Cheduba Islands, our surveys demonstrate that the upper growth limit of living oysters (e.g., *Saccostrea* spp.) occurs between mean higher high water (MHHW, ~1 m above MSL) and mean high-water spring (MHWS, ~1.3 m above MSL). This upper growth limit is slightly higher than documented elsewhere [e.g., *Kelletat*, 1988; *Beaman et al*., 1994; *Lewis et al*., 2008].

[17] In our area, living oysters commonly adhere to sandstone cliffs and isolated sandstone columns on wave-cut platforms. The vertical range of oyster growth overlaps with the zone of barnacle growth, but the highest barnacles are generally higher than the highest oysters, extending above MHWS. Because modern oysters in the littoral zone are easily collected by local fishermen, they rarely form prominent oyster encrustations, in stark contrast to older, fossil populations. Instead, they usually grow as individuals on rock surfaces. In locales not frequented by fishermen, we observed living oysters forming very dense belts beneath MHWS.

3.1.2. Coral Microatolls and Coral Heads

[18] In general, coral microatolls provide us with the most precise water-level indicators. Their upper growth limit develops between mean lower low water (MLLW) and mean low-water spring (MLWS) in the mesotidal environment (Figure 2). This is consistent with their being able to survive short periods of exposure above the sea during the lowest monthly tides. This relationship of the highest level of survival (HLS) of coral microatolls to low-tide levels has been used recently to document sea level history [e.g., *Chappell et al*., 1983; *Zachariasen et al*., 1999; *Natawidjaja et al*., 2007; *Kench et al*., 2009; *Meltzner et al*., 2010].

[19] Recent studies have shown that the relationship of HLS to low tides varies with tidal environments and coral species. In microtidal environments such as western Sumatra (maximum tidal range 0.8–1 m), HLS for massive species of the genus *Porites* is about 20 cm above extreme low water (ELW) [*Meltzner et al*., 2010]. For *Goniastrea retiformis*,

HLS is about 10 cm higher there. In mesotidal environments (with 2–6 m tidal ranges) such as the Great Barrier Reef, the uppermost level of living corals approximates MLWS [e.g., *Chappell et al*., 1983; *Hopley*, 1986], which is approximately 70 cm higher than ELW.

[20] Along coasts with tidal ranges similar to that of the western Myanmar coast (tidal range ~2 m), the HLS of microatolls is between MLLW and MLWS [*Kayanne et al*., 2007; *Kench et al*., 2009]. This elevation is similar to HLS on the Great Barrier Reef. In addition, we observed that the HLS of living coral in a semiconfined tidal pool is not higher than MLLW on northern Ramree Island, whereas the HLS of microatolls in open water environments must be lower than MLLW. Thus, it is reasonable to suggest that the HLS of the microatolls of western Myanmar is at an elevation that is similar to the microatoll HLS in other mesotidal environments and is not higher than the level of MLLW.

[21] Although the uplifted microatolls are a precise water-level indicator, well-preserved microatolls are rarely found in our field area. In places where we did not find microatolls, we compare the elevation of the highest coral colony to the current MLLW. This yields a minimum water-level change since the growth of corals.

3.2. Erosional Coastal Features

3.2.1. Shoreline Angles

[22] The term "shoreline angle" refers to the locus of points that form the join between a wave-cut platform and a sea cliff. Uplifted shoreline angles are one of the most common coastal features in our field area and have been widely used in coastal geomorphic studies to reconstruct histories of sea level change [e.g., *Hull*, 1987; *ten Brink et al*., 2006; *Saillard et al*., 2009]. In macrotidal and mesotidal environments, field observations suggest that they usually develop between MHWS and mean high-water neap (MHWN) [*Hull*, 1987]. In places where the tidal range is similar to our study area, modern shoreline angles develop in a more restricted position within this range, near the elevation of MHHW [*ten Brink et al*., 2006]. Our field surveys confirm that shoreline angles usually form in our area near MHWS, about 20 cm above MHHW. In rare cases, though, we found that the shoreline angle has developed a bit higher, above MHWS, perhaps due to erosion by waves during storm surges.

[23] Alluvial or talus deposits at the base of a sea cliff often obscure the shoreline angle. In such cases, the elevation of a shoreline angle would be overestimated unless it is dug out or exposed by erosion. Due to the very limited surveying time in the field, we did not try to dig the shoreline angle out while surveying the profiles. Instead, we extrapolated the terrace profile and the sea cliff slope to estimate the elevation of the shoreline angle to avoid the influence of later deposition.

[24] The uncertainties in our measurements of shoreline angle elevations are likely greater than our measurements of biological sea level indicators, due to both the obscuration by sediments on the wave-cut platform and the variability of the strength of storm surges. To account for these uncertainties and variability, we assumed that our shoreline angle measurements represent MHWS + 1 m in our study area.

3.2.2. Sea Notches

[25] We found two types of wave-cut notches: tidal notches and surf notches. Each of these is distinguished by its particular shape. Tidal notches are U- or V-shaped indentations that develop on cliffs or steep slopes in hard rock. They result from wave action as the tides bring the sea surface through the intertidal range. The deepest part of the indentation occurs at the level of mean sea level (MSL) [*Pirazzoli*, 1986]. In our area, tidal notches are most commonly cut into sandstone cliffs. They commonly have a gentle U shape, with the opening 1–2 m wide from the base of the U. Oysters and other marine organisms commonly grow within the notches.

[26] Surf notches exhibit far less erosional height than tidal notches in our study area. We commonly found modern surf notches at active shoreline angles and on sandstone platforms near MHWS, well above the tidal notches. These notches often form above the high tide where the cliff is regularly washed by waves [*Pirazzoli*, 1986]. Thus, unlike the tidal notches, their heights are related to the energy of the surf rather than to the tidal range.

[27] The accuracy with which marine notches reflect sea level varies depending on the tidal range, the geomorphology of the site, and the slope of the bedrock [*Pirazzoli*, 1986]. For example, along one short stretch of coast, we found that the elevation of a modern tidal notch on a sandstone ridge facing the open ocean is nearly 1 m lower than that on another part of the same ridge, but at the top of a sandy beach. This elevation difference is very likely the result of differing wave runups in these two different settings during tidal surges. Therefore, we suggest that the elevations of marine notches are uncertain by ± 1 m in our study area.

3.2.3. Wave-Cut Platforms

[28] Although modern and uplifted wave-cut platforms are the most common features along the coasts of Cheduba and Ramree Islands, they are not a precise sea level indicator in our study area. Wave-cut platforms generally develop within the intertidal zone and commonly extend below it, where bedrock can be eroded by wave action [*Trenhaile and Layzell*, 1981]. Along mesotidal coasts, the elevation of the platform may ramp 3–4 m from below low tide to high tide. Thus, a direct comparison of the elevation difference between a point on an uplifted platform and a point on the modern platform is not very useful in constraining uplift or subsidence. Since wave-cut platforms commonly develop between MHWS and MLWS, we suggest that their elevations generally indicate MSL $\pm$ half of the tidal range. This great uncertainty makes wave-cut platforms the worst sea level indicators in our study area. However, in places where no other indicator is available, and we were able to confirm the sediments are thin on the uplifted platform (i.e., <1 m), we estimated a minimal land-level change by measuring the elevation difference between the modern shoreline angle and an uplifted wave-cut platform.

4. Coastal Emergence

4.1. Ramree Island

[29] Ramree Island lies ~70 km east of the deformation front and is elongate parallel to the strike of the megathrust. This 80 km long, 20 km wide island is connected to the

mainland of Myanmar by a marsh that is slightly higher than the intertidal zone (Figure 1b).

[30] Our field observations on the island were limited by the availability of access roads. A semipaved road along the northern half of the island's western coast provides good access to its northwestern coastline, but the marshy northeastern part of the island is difficult to reach by car. Farther south, overland access is even more limited by the lack of roads. Therefore, we relied on chartered boats to sail to some larger towns on southeastern Ramree. Access to smaller villages along the southwestern coast was by foot. In places where chartered boats were unable to get close to shore, our observations were limited to views from offshore. These logistical difficulties significantly limited our ability to perform detailed, high-precision surveys along the southern coasts of Ramree Island.

4.1.1. Northern Ramree Island (Kyauk-Pyu Area)

[31] Ancient sea level indicators reveal that changes in land level differ greatly between northwestern and northeastern Ramree Island. Evidence for progressive uplift is abundantly clear in the former and absent in the latter. About 3 km west of Kyauk-Pyu (Figure 3), the largest city of the island, we found a series of uplifted tidal notches and bands of uplifted oysters on a sandstone ridge below the surface of the lowest marine terrace, T1 (KPU-15 in Figures 3 and 4). These stacked ancient coastal features indicate successive uplift events during the Holocene period.

[32] The lowest uplifted tidal notch is ~1.5 m above the modern notch. A layer of dead oysters encrusts the sandstone cliff slightly above the uplifted tidal notch and is ~1 m above the top of the band of modern oysters (Figure 4). A radiocarbon date from the dead oysters (assuming the global average marine reservoir correction) suggests that this oyster reef grew between 1417 and 1618 Common Era (C.E.) (Figure 4 and Table 1). This date is suspect because the local marine reservoir correction (Delta-R) is unknown. Nonetheless, this date is similar to other radiocarbon ages of uplifted corals and oysters north of Ramree Island [*Than Tin Aung et al.*, 2008]. Therefore, we believe that the uplifted oyster layer (KPU-15), together with the lowest uplifted tidal notch, was elevated during a regional tectonic event. The fact that the radiocarbon age is a century or two earlier than the great 1762 Arakan earthquake encourages the speculation that it was during this earthquake that this lowest notch and its associated oysters rose out of the intertidal zone.

[33] To the east, the magnitude of late Holocene emergence is much smaller. Fossil mid-Holocene coral microatolls south of Kyauk-Pyu rest upon the T1 surface, which is only slightly above the current MHWS (Figure 3). These microatolls are present from the terrace surface to the modern tidal flat, and the elevations of their upper surfaces are 1–1.5 m above MSL or 2–2.5 m above the current MLLW. U-Th analyses show that the ages of these corals range from 5000 to 7100 years B.P. (Table 2, KPU-102 to KPU-110). Both the ages and the elevations of these corals are consistent with the timing and water level of the mid-Holocene high stand of the eastern Indian Ocean [*Woodroffe and Horton*, 2005; *Briggs et al.*, 2008]. Thus, these corals suggest negligible net uplift of northeastern Ramree Island since the middle of the Holocene epoch.

[34] The broad morphology of Ramree Island reflects a northeastward tilt that is wholly consistent with the contrast in uplift between these two sites. A single, large, low terrace (T1) and a plexus of estuaries and tidal channels dominate the surface of the northeastern part of the island (Figure 3). In great contrast to this, flights of marine terraces dominate

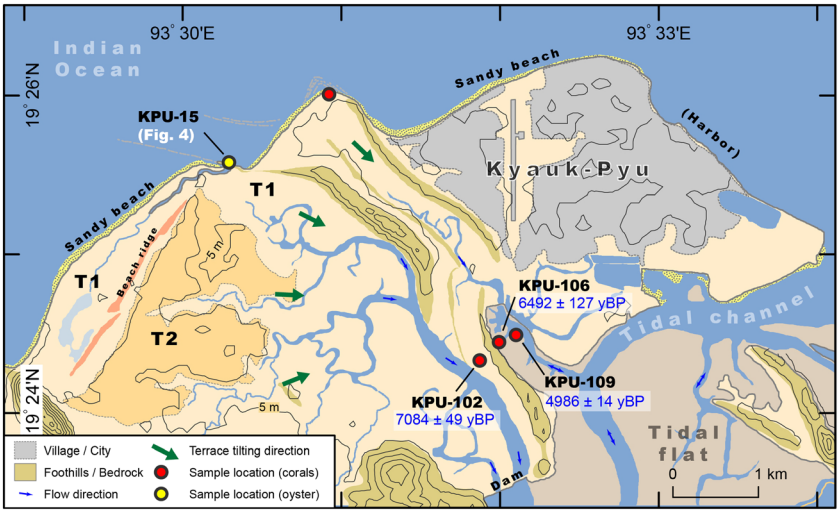

Figure 3. The patterns of marine terraces, current drainages, and tidal flats show the eastward tectonic tilting in northern Ramree Island over the past several thousand years. The geomorphic characteristics in the northwestern part of the island are very different from those in the northeastern part of the island. In the east, mid-Holocene fossil coral microatolls (KPU-102, KPU-106, and KPU-109) are present slightly above the modern high tide, reflecting a very small long-term uplift. To the west, however, a flight of wave-cut notches shows clear signs of long-term successive uplift, and the last uplift event occurred after the 16th century (KPU-15, Figure 4). Blue numbers show the U-Th age of the coral microatolls in years B. P. (yBP).

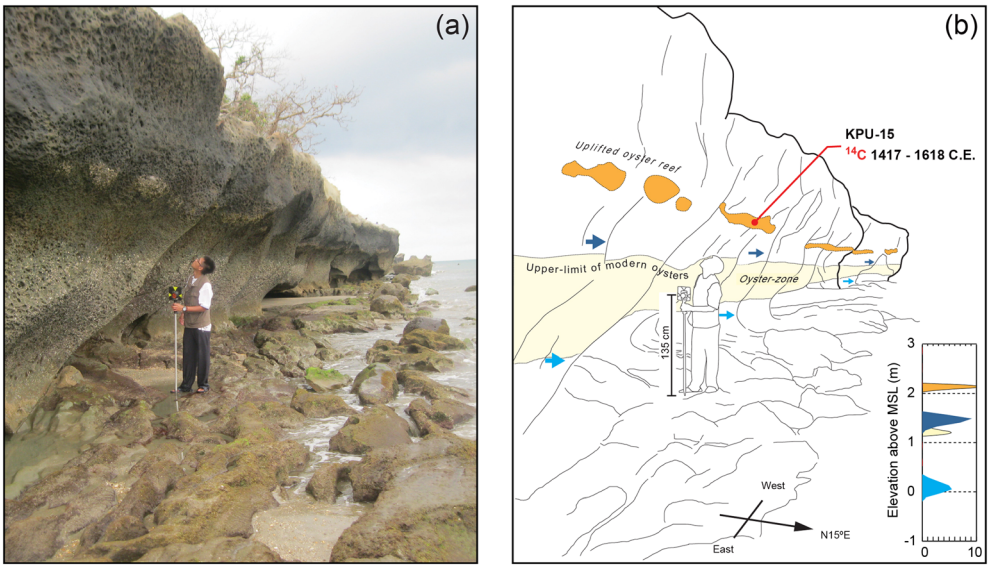

Figure 4. (a) Photograph and (b) line sketch of site KPU-15. Here a belt of uplifted oyster fossils and a wave-cut notch beneath T1 suggest about 1–1.5 m of land-level change since the 16th century. Several levels of higher wave-cut notches on a sandstone ridge at the same site suggest successive uplift events in the past several thousand years. The radiocarbon age of uplifted oyster fossils (KPU-15) above the lowest uplifted sea notch suggests that the last land-level change event occurred after the 16th century. The uplifted oyster fossils (shown in orange) are ~1 m above the modern oyster growth zone (shown in yellow). This elevation difference is similar to that between the modern sea notch (light blue arrows) and the uplifted sea notch (dark blue arrows). The elevation distributions of the oyster fossils and the wave-cut notch are shown in the inset of Figure 4b. The color code is the same as that in the line sketch.

Table 1. Radiocarbon Ages Obtained in This Study

Laboratory ID	Sample	Sample Type	Measured Age (B.P.)	$\delta^{13}C$ (‰)	Conventional Age (B.P.)	Calendar Year[a,b] (2σ) From		To
Northern Ramree Island								
Beta-285817	KPU-15	Oyster	420 ± 50	−0.10	830 ± 50	1417	to	1618
Eastern Cheduba Island								
Beta-301002	KK-145	Oyster	280 ± 40	−0.30	690 ± 40	1520	to	1686
Beta-301003	KK-146	Oyster	330 ± 70	−0.10	740 ± 70	1454	to	1685
Beta-301004	KK-148	Oyster	350 ± 40	−0.50	760 ± 40	1472	to	1647
Northwestern Cheduba Island								
Beta-301005	TY-140	Oyster	380 ± 40	0.70	800 ± 40	1447	to	1623

[a]Samples are calibrated using the modeled ocean average *Marine09* calibration curve [*Reimer et al*, 2009].
[b]We assume that $\Delta R = 0$ due to the lack of proper information along the eastern side of Bay of Bengal.

the geomorphology of the southwestern coast of the island. This contrast implies northeastward tilt of the island, with significant net uplift of the southwestern coast tapering northeastward to zero.

4.1.2. Central Ramree Island

[35] Uplifted corals and other sea level indicators demonstrate that the central western coast of Ramree Island rose several meters during the last emergence event, much more than that on the northwestern tip of the island. In situ fossil coral heads (ZC-16, ZC-118, and ZC-119) rest on a T1 surface that is ~3.5 m above MSL (Figures 5 and 6a). The fact that the highest upper surface of these corals is about 5 m above the current MLLW implies that they are now about 5 m above the modern highest level of coral growth. Farther inland are fossil oysters in growth position on bedrock of T1 that are about 5 m above their modern growth position (~MHHW; Figure 6a). These two sea level indicators demonstrate the land-level change since just before the last event is about 5 m along the central western coast.

[36] Samples from within the coral heads yielded very precise U-Th ages. All three heads were living in the middle decades of the 18th century (Table 2). Among these U-Th dates, the age of ZC-16 provides us the best timing constraint of the uplift event. There are four annual bands between the dated annual band and the outermost band, which represents the date of death of the coral. Thus, the coral appears to have died in 1762 ± 11 C.E., a perfect match for the 1762 earthquake. Although the growth bands are not as clear as the ZC-16 sample, the U-Th ages from the other two samples (ZC-118 and ZC-119) collected from

Table 2. U-Th Compositions and ^{230}Th Ages for Fossil Coral Samples of Myanmar by MC-ICP-MS

Sample ID	Type	^{238}U ppb		^{232}Th ppt		$\delta^{234}U_{initial}$ corrected[a,b]		$[^{230}Th/^{238}U]$ activity[c]		$[^{230}Th/^{232}Th]$ ppm[d]		Age Uncorrected		Age Corrected[c,e]		Age Years (B.P.)[f]		Calendar Year (C.E.)		
Northern Ramree Island																				
KPU-102a	*Coral remains*	2498	±2	2830	±12	148.9	±1.5	0.0731	±0.0002	1065	±5	7187	±24	7145	±49	7084	±49	−5183	to	−5085
KPU-103	*Coral remains*	2516	±2	2764	±9	149.9	±1.7	0.0736	±0.0002	1106	±5	7229	±26	7188	±48	7127	±48	−5226	to	−5129
KPU-104b	*Coral (Round)*	2490	±2	93	±7	148.9	±1.7	0.0669	±0.0001	29568	±2107	6561	±15	6559	±15	6498	±15	−4563	to	−4534
KPU-106	*Coral microatoll*	2505	±2	7273	±38	150.1	±1.6	0.0680	±0.0006	387	±4	6662	±65	6553	±127	6492	±127	−4669	to	−4415
KPU-107	*Coral microatoll*	2672	±2	5090	±13	149.7	±1.7	0.0667	±0.0003	578	±3	6532	±29	6460	±77	6399	±77	−4526	to	−4373
KPU-108	*Coral, overturned*	2673	±2	22559	±74	148.4	±1.7	0.0784	±0.0006	153	±1	7731	±63	7415	±323	7354	±323	−5727	to	−5081
KPU-109a	*Coral microatoll*	2730	±2	446	±7	147.9	±1.8	0.0519	±0.0001	5241	±84	5053	±13	5047	±14	4986	±14	−3050	to	−3022
KPU-110a	*Coral microatoll*	2625	±1	767	±7	150.8	±1.1	0.0634	±0.0001	3585	±33	6199	±15	6189	±18	6128	±18	−4196	to	−4159
Central Western Ramree Island																				
ZC-16a	*Coral*	3023	±3	899	±4	146.9	±1.6	0.0276	±0.00003	154	±2	264	±3	252	±11	192	±11	1746	to	1769
ZC-118a	*Coral microatoll?*	2929	±3	566	±7	149.0	±1.7	0.0287	±0.00004	245	±5	273	±4	266	±8	205	±8	1737	to	1753
ZC-119a	*Coral microatoll?*	2740	±4	1354	±8	151.4	±2.2	0.0296	±0.00005	99	±2	281	±5	263	±19	202	±19	1729	to	1767
ZC-119-1	*Coral microatoll?*	3332	±4	2316	±7	151.9	±2.0	0.0295	±0.00003	70	±1	280	±3	264	±9	203	±9	1738	to	1756
ZC-04	*Coral block*	3045	±3	604	±5.4	149.9	±1.5	0.0363	±0.00003	303	±4	346	±3	338	±8	278	±8	1664	to	1680
Southern Ramree Island																				
KYM-125a	*Coral*	2628	±3	716	±7	150.1	±1.8	0.0722	±0.0002	4378	±43	7094	±20	7084	±22	7023	±22	−5095	to	−5050
KYM-125b	*Coral*	2708	±3	1167	±7	150.0	±2.2	0.0748	±0.0002	2866	±19	7352	±23	7336	±28	7275	±28	−5353	to	−5297
KYM-127	*Coral*	2715	±3	710	±7	150.2	±2.0	0.0720	±0.0002	4546	±47	7068	±22	7058	±24	6997	±24	−5071	to	−5024
TK-130	*Coral block*	2957	±5	2707	±8	153.1	±2.5	0.0543	±0.00006	98	±1	515	±6	481	±35	420	±35	1495	to	1564
TK-131	*Coral block*	2933	±4	1042	±8	153.1	±2.2	0.0587	±0.00005	273	±3	557	±5	544	±14	483	±14	1453	to	1481
TK-132	*Coral block*	2861	±4	642	±7	154.6	±2.4	0.0747	±0.0002	5497	±61	7319	±25	7310	±26	7249	±26	−5326	to	−5273
Ka-Ma, Cheduba Island																				
KM-143a	*Coral remains*	2926	±4	905	±7	147.2	±2.2	0.0163	±0.00007	868	±8	1559	±8	1548	±14	1487	±14	449	to	477
KM-144a	*Coral microatoll*	2733	±4	1289	±7	146.9	±2.3	0.0063	±0.00005	221	±2	603	±5	585	±18	524	±18	1408	to	1445
Ka-I, Cheduba Island																				
KI-152a	*Coral microatoll*	2167	±3	3106	±10	149.2	±2.3	0.0030	±0.00006	35	±1	287	±6	233	±54	172	±54	1724	to	1832
KI-154a	*Coral microatoll*	2390	±4	1272	±7	146.9	±2.4	0.0115	±0.00007	356	±3	1097	±7	1077	±21	1016	±21	913	to	955
KI-155a	*Coral microatoll*	2140	±3	9038	±24	150.4	±2.7	0.0296	±0.0002	116	±1	2846	±23	2688	±160	2627	±160	−837	to	−517
KI-156a	*Coral*	1896	±3	534	±7	149.6	±2.5	0.0230	±0.00009	1350	±18	2210	±10	2199	±15	2138	±15	−203	to	−173
KI-157a	*Coral microatoll*	2339	±4	206	±6	148.3	±2.5	0.0078	±0.00005	1460	±44	745	±5	742	±6	681	±6	1263	to	1276
Sachet, Cheduba Island																				
SC-150a	*Coral remains*	2543	±4	206	±7	148.2	±2.2	0.0068	±0.00005	1395	±46	652	±5	649	±6	588	±6	1355	to	1368
SC-151a	*Coral*	3056	±5	1083	±7	149.6	±2.2	0.0142	±0.00006	662	±5	1359	±6	1346	±15	1285	±15	651	to	680
Man-Aung, Cheduba Island																				
MA-135	*Coral*	3142	±4	2056	±9	147.6	±2.1	0.0135	±0.00008	341	±2	1296	±8	1271	±26	1210	±26	714	to	765
MA-136a	*Coral, overturned*	2688	±3	2554	±9	145.2	±1.9	0.0145	±0.00009	252	±2	1394	±9	1358	±37	1297	±37	616	to	690
MA-136b	*Coral, overturned*	2633	±3	354	±7	148.9	±1.9	0.0145	±0.00006	1782	±34	1389	±6	1384	±8	1323	±8	619	to	635
MA-138b	*Coral*	2393	±5	1284	±7	147.6	±2.9	0.0138	±0.00007	425	±3	1323	±8	1303	±22	1242	±22	686	to	729

Analytical errors are 2σ of the mean.

[a] $\delta^{234}U = ([^{234}U/^{238}U]_{activity} - 1) \times 1000$.

[b] $\delta^{234}U_{initial}$ corrected was calculated based on ^{230}Th age (T), i.e., $\delta^{234}U_{initial} = \delta^{234}U_{measured} \times e^{\lambda 234 * T}$, and T is corrected age.

[c] $[^{230}Th/^{238}U]_{activity} = 1 - e^{-\lambda 230 T} + (\delta^{234}U_{measured}/1000)[\lambda_{230}/(\lambda_{230} - \lambda_{234})](1 - e^{-(\lambda 230 - \lambda 234)T})$, where T is the age. Decay constants are 9.1577×10^{-6} year^{-1} for ^{230}Th, 2.8263×10^{-6} year^{-1} for ^{234}U [*Cheng et al.*, 2000], and 1.55125×10^{-10} year^{-1} for ^{238}U [*Jaffey et al.*, 1971].

[d] The degree of detrital ^{230}Th contamination is indicated by the $[^{230}Th/^{232}Th]$ atomic ratio instead of the activity ratio.

[e] Age corrections were calculated using an estimated atomic $^{230}Th/^{232}Th$ ratio of 6.5 ± 6.5 ppm [Zachariasen et al., 1999].

[f] Years before present (B.P.) is referenced to 1950 C.E.

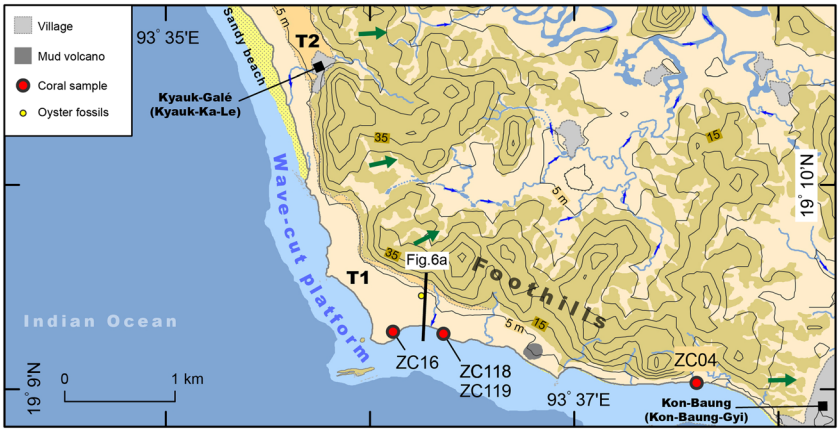

Figure 5. The patterns of modern drainages and marine terraces of the central western coast of Ramree Island also show an eastward tilt. The fluvial plain and terraces northeast of the foothills show clear eastward tilting in the analysis of aerial photos and drainage patterns. West of the foothills, the elevation of the lowest terrace between the villages of Kyauk-Ka-Le (Kyauk-Galé) and Kon-Baung-Gyi (Kon-Baung) was described by *Mallet* [1878] to be ~6 m above the water level at the time of his visit.

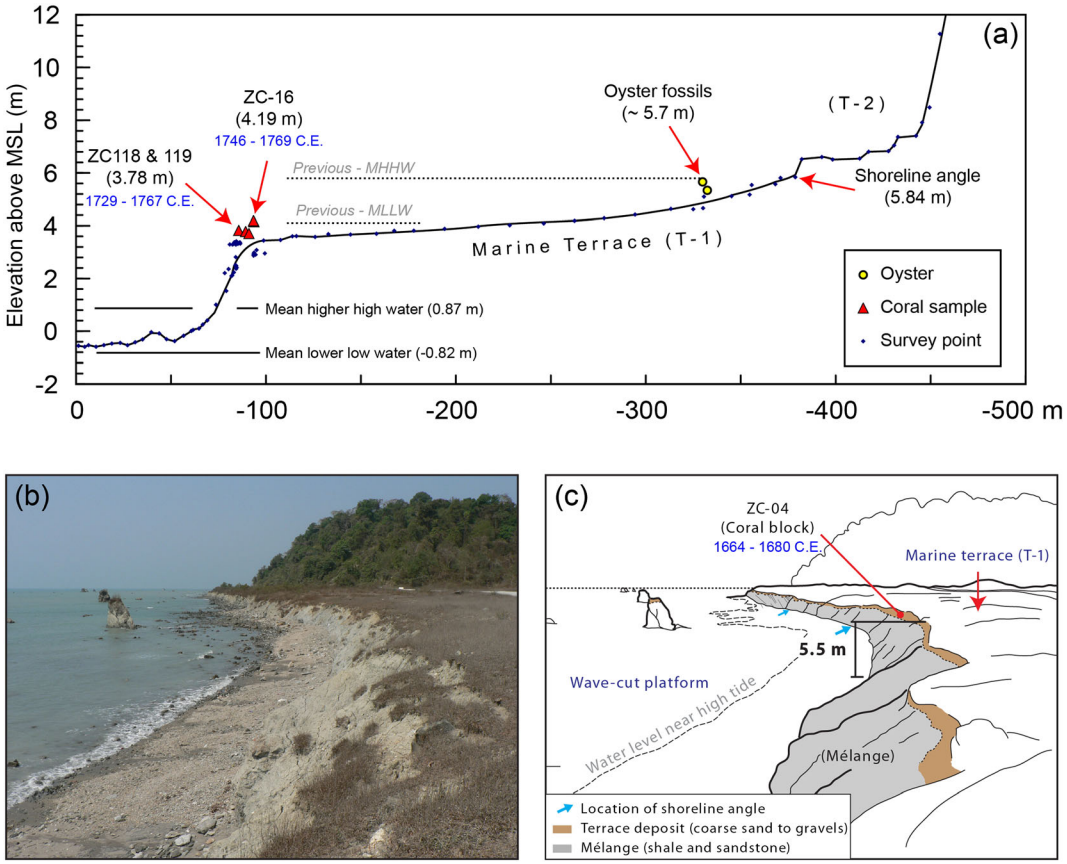

Figure 6. Our field survey sites at the central western Ramree coast. (a) The U-Th ages of uplifted coral microatolls on the lowest terrace (T1) show that ~5 m of land-level change occurred in the 18th century, most likely during the 1762 earthquake. The profile location is indicated in Figure 5. All sea level indicators on T1 show identical amount of land-level change relative to their equivalent tide-water level. (b) Photograph and (c) line sketch of site ZC-04. Here a dated coral block within the terrace deposits of T1 also indicates that an uplift event occurred after the 17th century. The terrace surface elevation at ZC-04 is higher than that at the previous site (ZC-16), at 5.5 m above the modern shoreline angle. This yields the minimal amount of land-level change at ZC-04. However, both the amounts at ZC-16 and ZC-04 are lower than the 19th century account of *Mallet* [1878].

the band further inside the colonies also yield a date of death very close to 1762 C.E. (Table 2). This also implies that the T1 wave-cut platform on the central western coast formed long before 1762, then supported coral growth through the decades before the uplift in 1762.

[37] This extraordinary amount of land-level change along central western section of Ramree Island attracted attention as early as the mid-19th century. This is where *Mallet* [1878] observed a "raised beach about 20 feet above the sea" during his survey in 1877. Following the description and the map in his report, we were able to survey the same section of the coast between the villages of Kyauk-Ka-Le (Kyauk-Galé) and Kon-Baung-Gyi (Kon-Baung; Figure 5). We found the surface of T-1 there is 5.5 m above the current shoreline angle, with a very thin sedimentary cover (Figure 6b). Although this is our highest measurement along this section of the coast, it is slightly lower than Mallet's observation in 1877. The 17th century age of a coral fragment (ZC-04) within the thin sediments is consistent with the terrace being an active wave-cut platform a century or so before the uplift in 1762 (Figure 6b and Table 2).

[38] Geomorphological evidence of a progressive northeastward tilt is even clearer for central Ramree Island than it is for the northern sector of the island. Along most of this section of coast, two to three major terrace treads along the southwestern coast contrast with only one major terrace in the northeast (Figure 5). Moreover, the highest terraces of the southwestern foothills show clear northeastward tilting of their surface in stereoscopic aerial photos. This eastward tilt is also consistent with the predominance of northeastward-flowing drainage networks over much smaller creeks flowing to the southwestern coast, similar to what have been observed on Makira (San Cristobal) Island, the Solomon Islands [*Chen et al.*, 2011]. The northeastward tilt of both the northern and central sectors of Ramree Island and the increase in uplift from the northern to the central western coast indicate the tilting results from the growth of the doubly plunging anticline that has raised the island (Figure 1).

4.1.3. Southern Ramree Island

[39] Geomorphic evidence for young land-level changes at the southern tip of the southwestern Ramree coast is also very clear, although the timing of the last uplift event is not as well constrained. A flight of marine terraces between the current shoreline and the western foothills indicates progressive uplift near the small village of Tet-Kaw (Figure 7). The amount of the last emergence is well constrained by the elevation of T1's shoreline angle, which is about 1.4–2 m above its modern analogue at MHWS. The elevation of a group of small surf notches on a sandstone ridge is similar to that of the shoreline angle (Figures 8b and 8c). These features suggest a smaller uplift, only 1.4–2 m from the current MHWS.

[40] A lack of datable in situ materials associated with the T1 surface precluded determination of a date for the most recent uplift in this area. Agricultural activities appear to have removed most of the fossil corals and oysters from the terrace. Nonetheless, several loose coral blocks within the thin sediment cap of T1 provide some constraint. These coral blocks are 10–30 cm in diameter, significantly bigger than regular beach gravels (<5 cm) within the modern storm deposits. Thus, it is unlikely that they were transported by normal storms or cyclones up onto the T1 surface after its emergence. Moreover, because we did not find any evidence of tsunami deposits along the coast, we believe that these coral blocks are not tsunami deposits, but were deposited when the T1 surface was still the active wave-cut platform. Thus, the youngest age of these coral blocks may represent the maximum age of the formation of T1.

[41] The U-Th ages of these coral blocks range from early mid-Holocene to the 16th century (Table 2, TK-130 to TK-132). The youngest U-Th age (1495–1564 C.E.) provides a maximum limiting age for wave action on T1.

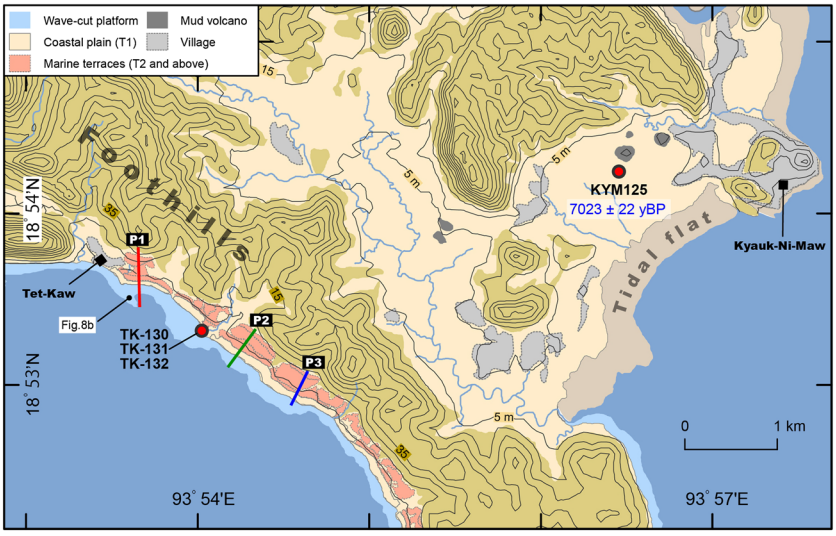

Figure 7. The different geomorphic characteristics of the southwestern and southeastern Ramree coast indicate the long-term uplift and eastward tilt of southern Ramree Island. Similar to the northeastern Ramree coast, the U-Th age of fossil corals on T1 (KYM-125) suggests that the lowest terrace formed during the mid-Holocene period. However, the geomorphic characteristics west of the foothills are very different. A flight of marine terraces along the western coast suggests successive uplift during the past thousands of years. Colored lines are topographic profiles across these marine terraces shown in Figure 8a. Red dots show the locations of dated corals.

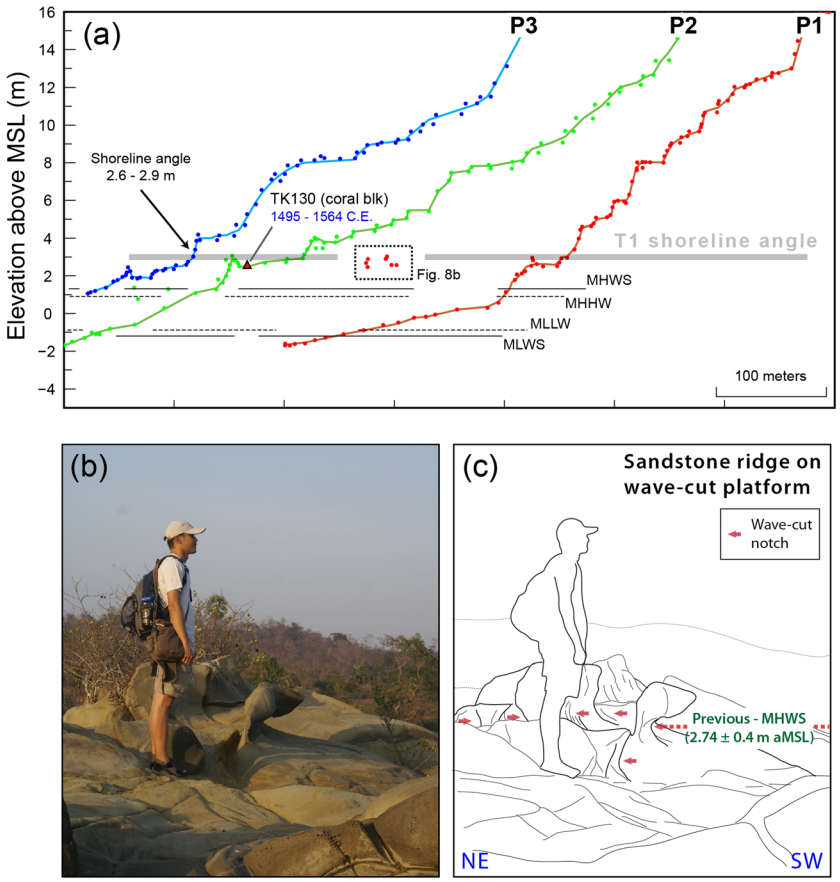

Figure 8. (a) Three topographic profiles at southwestern Ramree Island show ~1.5 m of land-level change of T1 after mid-16th century. The shoreline angle of T1 is about 1.5 m above its equivalent position in the modern tidal range. U-Th ages of coral blocks in the terrace deposits of T1 (e.g., TK-130) suggest that the uplift event occurred after mid-16th century. (b) Photograph and (c) line sketch of a series of small uplifted surf notches on an offshore sandstone ridge near profile P1. The location of this photograph is shown in Figure 7. These notches show the same amount of uplift as the shoreline angle of T1. The elevations of these small surf notches are ~1.5 m above the modern MHWS, where the modern shoreline angles and surge notches develop (see Figure 2).

Providing we are correct in deducing that this block is not a tsunami block, this age implies emergence of the T1 surface after the 16th century. We propose that the 1.4–2.0 m obtained from the sea level indicators of T1 represents the net uplift during and subsequent to 1762 here.

[42] The geomorphological contrast between the east and west facing coasts of the southern Ramree Island is like the contrast of the northern and central coasts. A flat, low T1 terrace dominates the southeastern part of the island, but its eastward tilt is not as prominent as it is across the northwestern and central sectors of the island (Figure 7). The shoreline angle of T1 near the village of Kyauk-Ni-Maw suggests that its corresponding MHWS is ~4 m higher than current MHWS. We found no in situ biological sea level indicators on the T1 surface, but we did find a group of small coral heads within the T1 terrace deposits that provide a plausible age for T1 (e.g., KYM-125 in Figure 7). Most of these heads are ~60 cm in diameter. The three U-Th ages obtained from two of the corals are consistent and suggest that the terrace formed sometime after 7300–7000 years B.P. (Table 2, KYM-125a/b and KYM-127). Although these corals are slightly older than the mid-Holocene ones on northeastern Ramree Island, their ages are still close to the timing of the mid-Holocene high stand in this region [*Woodroffe and Horton*, 2005]. Thus, the only plausible interpretation is that T1 near Kyauk-Ni-Maw formed during the mid-Holocene high stand. The lack of other uplifted features between the mid-Holocene terrace (T1) and the modern coast suggests that the land-level change must be very small since the mid-Holocene, less than ~4 m over the past 7000 years if we assumed that the sea level has been stable through the mid-Holocene to present.

4.1.4. Eastern Ramree Island

[43] In the lowlands of eastern Ramree Island, we found no good evidence for any young uplift event. Sea level indicators, where present, are barely higher than the current high-tide level. Both remote and field investigations revealed only one coastal plain surface between the modern shoreline and the foothills of eastern Ramree Island. Sandstone platforms and surf notches emerge above the water during low tides, but their elevations are not significantly higher than high-tide levels.

[44] We found one site with sea notches and associated shoreline angles higher than the modern high-tide level

(Figures 1 and 9). This site is at the end of a sandstone ridge and exhibits one sea notch and one shoreline angle, at elevations ~4 and ~2 m above the current MSL, respectively. Since this site is very difficult to access, we were not able to determine the elevation of the notches accurately, nor did we find any datable materials at this site to constrain their ages. However, because the ~4 m elevation of the higher sea notch above MSL is almost identical to the elevation of T1's shoreline angle near Kyauk-Ni-Maw, we speculate that this higher notch also formed during the mid-Holocene high stand and that the net uplift since the mid-Holocene is very similar in these two places.

[45] A lower surf notch and the associated shoreline angle ~0.7 m above MHWS may represent slight uplift, but these could also be active, modern features, given our uncertainty in high-water spring level here. When we visited this site during low tide, we noticed that the recent high-water mark was slightly higher than this lower shoreline angle, which suggests the water can reach the lower shoreline angle at least during the very high water period. Moreover, we did not find any other shoreline angle lower than this that may represent the modern shoreline angle. Judging from both lack of promising active shoreline angles matching to the elevation of MHWS, and the uncertainty of the shoreline angle's elevation (MHWS to MHWS + 1 m), we therefore suggest that the amount of land-level change here from the last event is smaller than the uncertainty of the sea level indicator, i.e., less than 1 m.

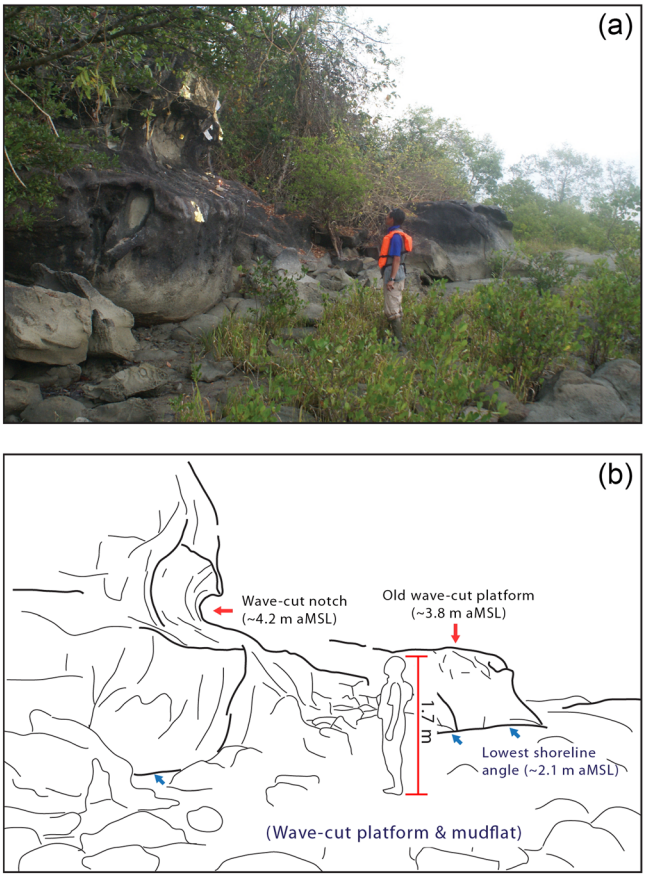

Figure 9. (a) Photograph and (b) line sketch of an inferred mid-Holocene wave-cut notch and wave-cut platform on the southeastern coast of Ramree Island. The location of this photograph is shown in Figure 1b. The wave-cut notch is ~4 m above the current MSL. Its elevation is similar to the elevations of mid-Holocene corals in northeastern and southeastern Ramree Island. Below the inferred mid-Holocene notch, the lowest preserved shoreline angle in the area is ~2.1 m above MSL. This implies <1 m of land-level change. See text for discussion.

4.1.5. Summary of Ramree Island

[46] In summary, all of the features that indicate young uplift of Ramree Island are along the western coast. There is clear evidence that the last big uplift occurred during the 1762 earthquake and that the greatest amount of uplift was at least ~5.5 m along the central western Ramree coast. The amount of uplift diminished northwestward and southeastward to only 1–2 m. We found no significant uplift associated with the 1762 earthquake along the northeastern coast of Ramree Island. Moreover, even mid-Holocene features are no more than ~4 m above their modern analogues. Because sea level in the mid-Holocene was likely a few meters higher than modern sea level, this likely indicates that uplift of the northeastern coastlines has been no more than a meter or so in the past 7 millennia. The elevation of these mid-Holocene features also implies that the swampy northeastern coast has not been subsiding over the past several thousand years.

4.2. Cheduba Island

[47] Between Ramree Island and the deformation front is Cheduba (Man-Aung) Island (Figure 1b). Its greater proximity to the deformation front (35–60 km) implies that it would experience greater uplift during a conventional megathrust earthquake. The longest dimension of Cheduba Island is ~30 km, but this is merely the exposed part of a ~140 km long doubly plunging submarine ridge that strikes parallel to the deformation front. The topography of the island and the submarine ridge is highly asymmetrical, with the southwestern flank being significantly higher, steeper, and more rugged than the northeastern flank (Figure 1b).

[48] Unlike Ramree Island, a semipaved road encircles the entire Cheduba Island, providing good access to its coasts. We surveyed five representative coastal sections around the island during our short visit.

[49] In general, our surveys confirmed Captain Halsted's early 19th century observations that large uplifts occurred along the western coast of Cheduba in 1762 [*Halsted*, 1841]. We also surveyed land-level changes along the island's eastern coast, where fewer previous terrace observations exist [e.g., *Brunnschweiler*, 1966]. Broadly speaking, our observations show that all of Cheduba Island rose during the last major uplift event, up to ~4 m along its western coast and ~1 m along its eastern coast.

4.2.1. Northwestern Cheduba Island (Ka-Ma Village)

[50] Figure 10 shows the distribution of marine terraces near the village of Ka-Ma, along the northern southwestern coast of Cheduba Island. Here we were able to map more than five terrace treads between the foothills and the current coastline, as reported previously by *Brunnschweiler* [1966] and *Shishikura et al.* [2009]. These terraces are mainly uplifted wave-cut platforms, cut into mélange or highly deformed sandstone and shale. A ~1 m thick bed of reef fragments, including clastic debris and in situ corals, mantles

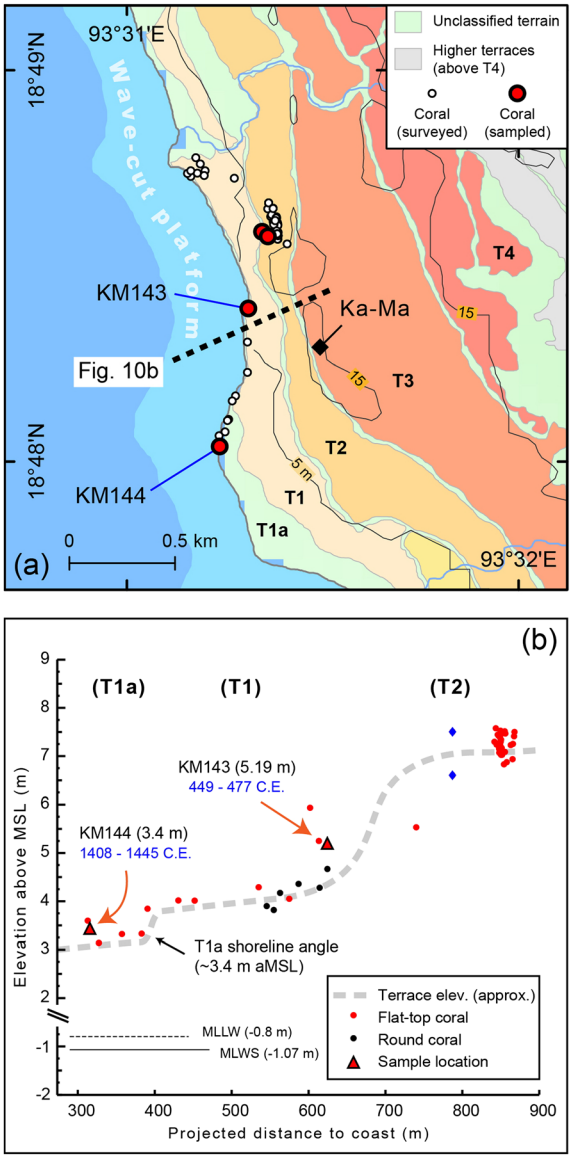

Figure 10. (a) The flight of marine terraces along the western coast of Cheduba Island near the village of Ka-Ma shows successive uplift. The geomorphic interpretations on this and following figures are based on analysis of nonstereoscopic high-resolution satellite imagery. See text for detailed discussion. Black dashed line indicates the approximate location of the topographic profile in Figure 10b. (b) The U-Th age of an eroded coral microatoll (KM-144) on the lowest terrace (T1a) suggests ~4.2 m of land-level change after the mid-15th century. The elevation difference between T1a and T1 is ~0.6 m. The U-Th age of KM-143 is discussed in the text. The elevations of the terraces are inferred from the surveyed coral elevations.

the bedrock platform of the lowest terrace (T1). Microatolls and corals with flat erosional surface on top (pseudomicroatolls) are present along the seaward edge of the T1 surface. Some of these emerged coral fossils have fallen to the current wave-cut platform during the erosional retreat of the modern sea cliff. Most of these fallen blocks appear along the current high-tide mark below the sea cliff.

[51] The elevation of T1 is about 3–4 m above MSL, but southwest of Ka-Ma, we can separate it into two subterraces (T1 and T1a) based on nonstereoscopic satellite images. Field measurements show that the lower terrace, T1a, is ~0.6 m lower than T1 (Figure 10b).

[52] The coral morphology and their U-Th ages reveal a complicated coral emplacement history of the lowest terraces (T1 and T1a). Coral colonies exist all over T1 from its seaward side to near its shoreline angle. Close to the terrace riser between T1 and T2, field measurements show that the elevation of a group of rounded corals is significantly higher than the elevation of microatolls along T1's seaward side (Figure 10). Although some of these rounded heads seem to retain their normal position, others are highly eroded. This situation is very similar to that at the current coastline where we found the fallen coral heads from the T1a terrace to the present wave-cut platform. Therefore, we suggest these high and rounded heads were dropped onto T1 while T1 was the active shore platform.

[53] Sample KM-143, from a massive coral block, yielded a very old age for one of these high coral heads, around 449–477 C.E. (Table 2). This age for one of the fallen blocks gives an age that predates the cutting of T1.

[54] Another coral sample from a microatoll on the lower T1a surface constrains the maximum age of the last-uplift event near the Ka-Ma village. Along the modern sea cliff, we found another group of microatolls on the surface of T1a, separated from T1 by a ~0.6 m high terrace riser (Figure 10b). These microatolls are slightly eroded and tilted and are close to the shoreline angle of T1a. Due to our very limited time in the field, we did not dig these microatolls out to confirm if they are in situ or displaced. However, we speculate that they were dropped from the original T1 surface to the lower T1a during the landward erosional advance of T1a's shoreline angle. This interpretation is consistent with their slightly eroded nature, their tilt, and their location on T1a, very near the uplifted T1 terrace riser.

[55] The other hypothesis is that those microatolls grew on the higher part of the platform while the platform was submerged by interseismic subsidence. However, if this were the case, the shoreline angle itself would have been also modified due to the easily eroded nature of the soft mélange bedrock materials. Such evidence does not appear along this small terrace riser between T1 and T1a. Thus, these microatolls predate the emergence of T1a.

[56] The U-Th age of sample KM-144 from one of these microatolls suggests that the emergence of T1a occurred no earlier than 1409–1445 C.E. (Table 2). This age allows the speculation that T1a emerged during the 1762 earthquake.

[57] The amount of land-level change from 1762 to now, however, is not well constrained at this location. The top of the microatolls (e.g., KM-144) that is very close to the T1a shoreline angle suggests at least 4.2 m emergence from the mid-15th century to now. On the other hand, the shoreline angle of T1a itself is only ~2.2 m above the current MHWS at the same location. These led us to suggest that the emergence from 1762 to now must be between 4.2 and 2.2 m at this location, where the mid-19th century account from Captain Halsted suggests about 4.5 m (16 ft) uplift [*Halsted*, 1841].

4.2.2. Southwestern Cheduba Island (Ka-I Area)

[58] The coral microatolls near the village of Ka-I provide the best constraints on land-level change during the 1762

earthquake along the southwestern coast of Cheduba Island. In this area, we were able to identify about four major terrace treads from nonstereoscopic satellite imagery (Figure 11). The lowest terrace, T1, is about 2–4 m above MSL. Uplifted coral colonies, especially coral microatolls, are abundant on the lower portion of the T1 surface. The tops of these microatolls are ~3.4 m above current MLLW. This difference represents the minimum uplift during and subsequent to the most recent large event. This number is very close to the ~3.6 m value reported from the southern end of Cheduba Island by *Halsted* [1841].

[59] Among these uplifted coral microatolls, we collected one sample (KI-152) from a giant (~4 m in diameter) microatoll for U-Th dating. The sampled annual band is few centimeters from the microatoll's noneroded perimeter. Its U-Th age indicates that the coral died sometime between 1724 and 1832 C.E., a period that includes the date of the 1762 earthquake (Table 2).

[60] Around the giant microatoll (KI-152), we found several smaller coral microatolls whose upper surfaces display evidence for slowly rising sea level during their growth. This "up-grown morphology" of *Hopley* [1986] or the "cup-microatoll" morphology of *Zachariasen et al.* [2000] is common above the Sunda megathrust in Sumatra, where the fore-arc islands slowly submerge during the interseismic period and then rapidly uplift during giant earthquakes [e.g., *Natawidjaja et al.*, 2007].

[61] In order to constrain long-term uplift rates in this area, we also collected several U-Th samples from corals at higher elevations (Figure 11). The highest coral sample (KI-156) is from a coral on the surface of T3, 11.4 m above current MLLW. U-Th analysis yielded an age of about 2100 years B. P. (Table 2). A sample (KI-155) from a coral microatoll on T2 (8.5 m above MLLW) yielded an age of about 2600 years B.P. Another coral microatoll near T1's shoreline angle (4.5 m above MLLW) yielded a U-Th age of 913–955 C. E. Although one of these dates is out of sequence, taken

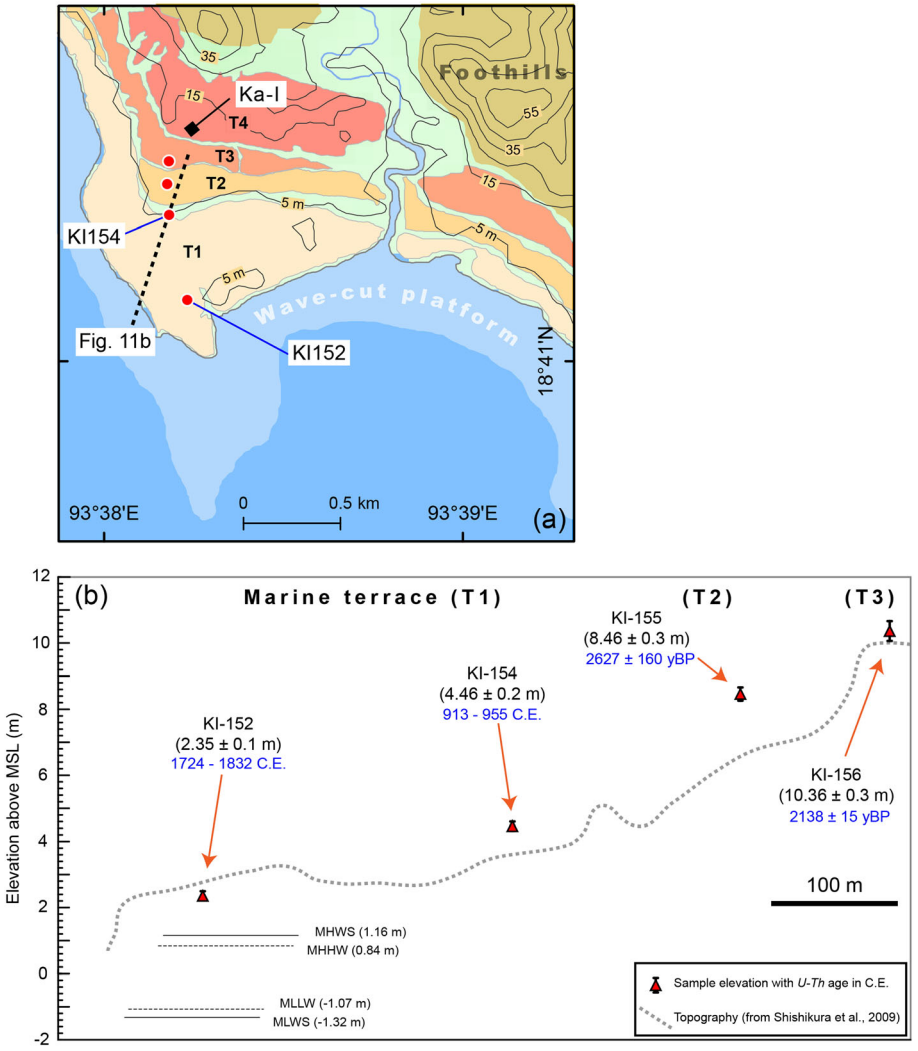

Figure 11. (a) Map and (b) topographic profile of marine terraces near the village of Ka-I at the southern tip of Cheduba Island. Here the flight of terraces shows progressive late Holocene uplift of the coast. The U-Th age of a coral microatoll (KI-152) on T1 shows ~3.4 m of land-level change after 1724–1832 C.E., most likely during the 1762 earthquake. See text for detailed discussion.

together, they suggest a late Holocene average uplift rate of about 3–5 mm/yr.

4.2.3. Eastern Cheduba Island (Kan-Daing-Ok Area)

[62] The magnitude of the most recent large uplift event decreases significantly from the southwestern to the northeastern side of Cheduba Island. This is evident in terrace elevations. Along the southeastern coast, the seaward edge of T5 coincides with the 15 m contour extracted from SRTM data (Figure 12). However, along the southwestern coast, the seaward edge of T4, rather than T5, follows the 15 m contour line (Figures 10 and 11).

[63] Along the southeastern coast, we surveyed two separate profiles to constrain recent land-level changes (Figure 12). Near the northern profile, modern erosion of the coastline exposes the stratigraphy beneath both T1 and T2. In each case, sediment mantling the wave-cut platform is less than 30 cm. Therefore, the topographic profile here approximates the shape and elevation of these wave-cut platforms. Here the topographic profile shows that the shoreline angle of T1 is ~1.1 m above the current MHWS (Figure 13a). Oyster and barnacle encrustations are abundant on in situ sandstone blocks near the elevation of the shoreline angle of T2 (~8.5 m above MSL). These encrustations and T2's shoreline angle emerged during an event prior to the uplift of T1. Radiocarbon analyses of these fossils suggest an age for T2 that ranges from the mid-15th to the late 17th century (Table 1, KK-145 to KK-148). Since the emergence of the T2 surface must be earlier than the formation of T1, the emergence of T1 occurred after the 15th century. Thus, we believe T1 at this location rose out of the water during the 1762 earthquake and is contemporaneous with the youngest terraces on the southwestern coast of the island.

[64] Three kilometers farther south along the coast, we constructed another topographic profile just south of the village of Kan-Daing-Ok (Figure 13b). Our analysis of nonstereoscopic satellite imagery suggests that all of T1 has been eroded away there. Along the modern shoreline, we found a group of highly eroded, massive, and displaced coral heads, the upper surfaces of which are at elevations near current MHHW, similar to the situation south of the Ka-Ma village. We believe that these corals grew near the seaward edge of a raised terrace (T2 or T1) and tumbled into the modern intertidal zone during the erosion of the modern sea cliff into the higher terrace. Although the elevations of these corals can no longer be used to constrain the amount of uplift since they died, their ages may still help us constrain the timing of the most recent large uplift event.

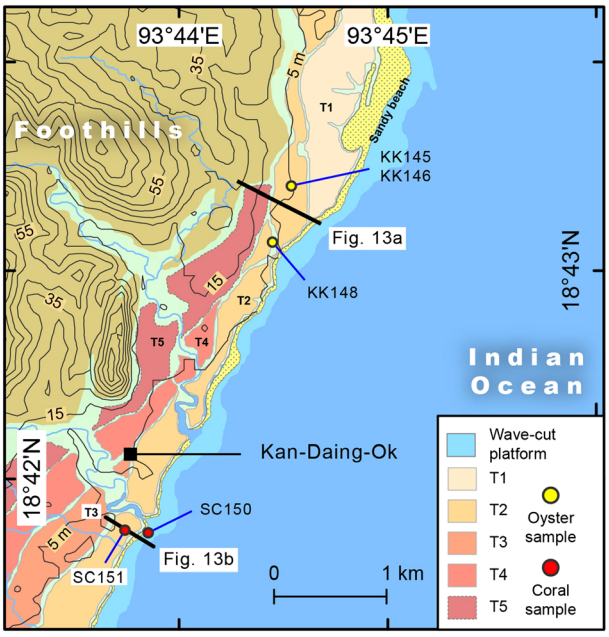

Figure 12. Map of the topographic profiles and sample locations on the marine terraces along the eastern coast of Cheduba Island.

[65] We collected a sample from one of these corals (SC-150) and another from the highest coral head that rests on the T2 surface (SC-151) for U-Th analysis. The fallen coral on the modern platform grew around 1355–1368 C.E., but the coral on the T2 surface was growing in the period between 651 and 680 C.E. (Table 2). Both of these samples antedate the 1762 earthquake, so any uplift associated with the 1762 earthquake must be smaller than the elevation of SC-151, i.e., less than 5 m.

[66] In fact, if the lower coral were displaced from the eroded surface of T2, the amount of emergence would be much less than 5 m. We analyzed the relationship between elevations of T2's shoreline angle and the coral heads. The higher coral's elevation (~4 m above modern MSL) is very close to the altitude of T2's shoreline angle (~4.5 m above MSL according to *Shishikura et al.* [2009]). This elevation difference is much smaller than the modern tidal range (~2.3 m) and suggests that the fossil coral and the shoreline angle are contemporaneous. Thus, either the higher coral lived prior to the formation of T2's shoreline angle and was displaced to its current position, or the coral grew after the development of the shoreline angle during the interseismic subsidence. Here we prefer the former interpretation because if the coral grew after the formation of the shoreline angle, we would expect the shoreline angle to be modified by later erosion of the soft mélange bedrock. On the other hand, if we extend the surface trend of T2 to the place above SC-150, the elevation of this extended T2 surface would be 2–2.5 m lower than T2's shoreline angle, which matches the modern tidal range (~2.3 m, Figure 13c). Therefore, it is reasonable to suggest that the U-Th age of SC-150 represents the age of T2. As a result, the amount of emergence from 1762 C.E. to present at this location has to be smaller than 3.3 m, which is the elevation from T2's shoreline angle to the current MHWS.

4.2.4. Northeastern Cheduba Island (Man-Aung Town Area)

[67] Terrace elevations at the northeastern tip of Cheduba Island are significantly lower than those along the western coast. For example, the surface of T3 in this area coincides with the 5 m contour line extracted from SRTM data (Figure 14a), whereas T3 along the southwestern coast is about 10 m above MSL. This implies that long-term net uplift diminishes from southwest to northeast across the island. Evidence along the modern coast also suggests relatively small net uplift in the northeast during the late Holocene epoch.

[68] North of Man-Aung Town, the main settlement of Cheduba Island, is a low sandstone ridge. Beneath the encrustations of modern oysters, but within the modern intertidal zone, are fossil coral heads. The elevation of these

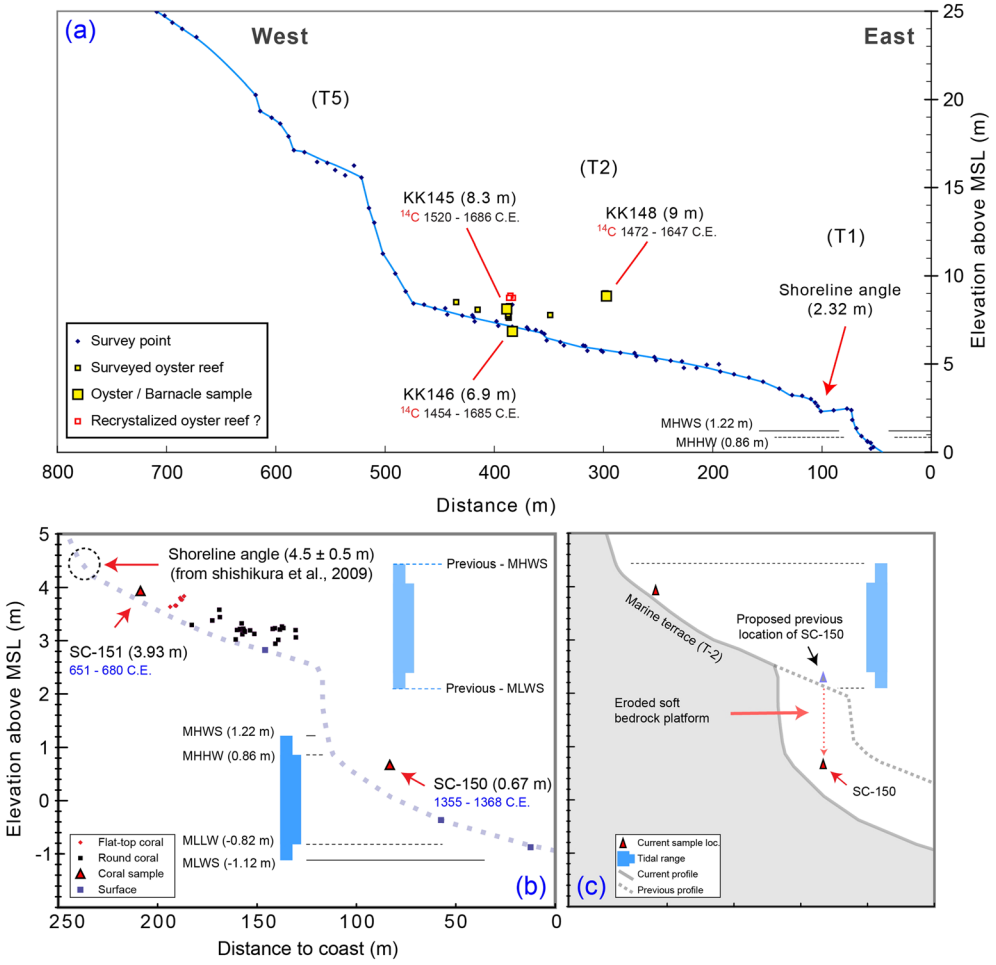

Figure 13. (a) A topographic profile north of the village of Kan-Daing-Ok (the location of the profile is shown in Figure 12). Here uplifted shoreline angle and oyster reefs show ~1.1 m of land-level change after the 17th century. The 15th to 16th century radiocarbon ages of the oysters on T2 suggest that the lowest terrace (T1) formed after the 17th century, likely during the 1762 earthquake. (b) The shoreline angle of T2 and the U-Th age of an eroded coral (SC-150) near the modern high tide suggest 1.5 to ~3 m of land-level change after the 14th century south of Kan-Daing-Ok. The topography profile and the elevation of the shoreline angle are modified after *Shishikura et al.* [2009]. The location of this profile is shown in Figure 12. (c) A proposed differential erosion model to interpret the elevation of sample SC-150. See text for discussion.

fossil corals, ~20 cm above MLLW, indicates that they have risen slightly above their modern maximum growth limit. U-Th analyses of three samples show that all grew in the 7th and 8th centuries (Table 2, MA-135, 136, and 138). Unfortunately, these coral colonies are not microatolls, so they could have grown substantially below MLLW. Nonetheless, their elevations above MLLW suggest very little emergence in the past 1400 years.

[69] Elevation differences between the modern beach berm and an ancient one provide a better estimation of uplift in 1762 here. Near the coral fossils, the modern beach berm (on the seaward edge of T1) is 0.8 ± 0.2 m below another beach berm (on the seaward edge of T2). These two berms sit in nearly identical environments with respect to the ocean, so it is reasonable to argue that their elevation difference reflects the net uplift between the time of formation of the older berm and the present. We did not find datable materials to constrain the age of the uplifted beach berm, but we propose that it was raised during the 1762 earthquake.

4.2.5. Northwestern Cheduba Island (Taung-Yin Area)

[70] At the northern tip of Cheduba Island, an unusually wide and high T1 surface lies between the modern coastline and the foothills (Figure 15). On high-resolution satellite imagery are two obscure terrace risers that cut obliquely across this wide terrace, separating it into three subterraces (T1a, T1b, and T1c). These two terrace risers are not apparent in the topographic profile that we surveyed in the field (Figure 15b), perhaps because of our choice of location for the survey or because of agricultural modifications. Slight undulations in curvature along the surveyed profile of T1 suggest, however, that the higher and lower portions of T1 may not have formed at the same time.

[71] Near the highest portion of T1, at about 7.3 m above MHHW, are fossil oysters that encrust an isolated sandstone

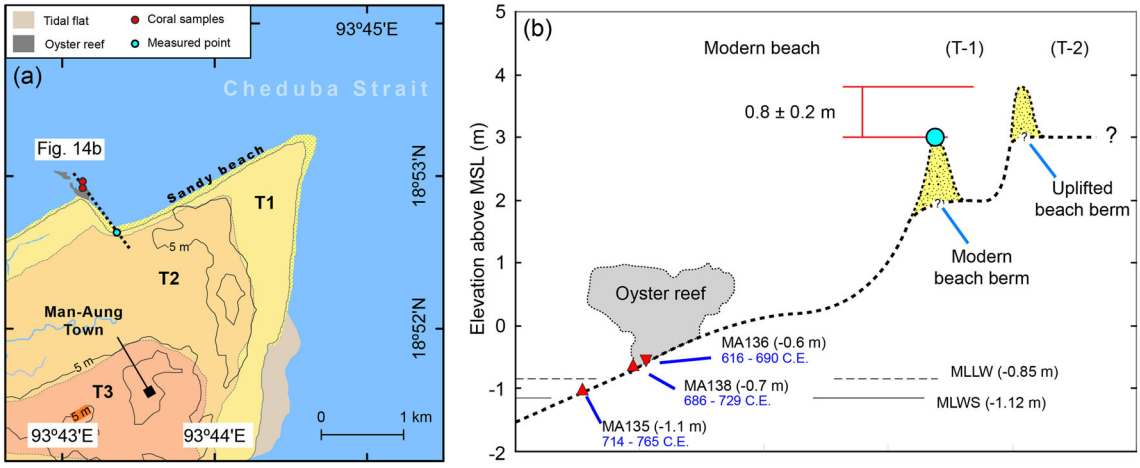

Figure 14. (a) Marine terraces at the northeastern tip of Cheduba Island are lower than their equivalents along the western Cheduba coast. The elevation of T2 near Man-Aung Town is less than 5 m from the contour of SRTM data set [*Jarvis et al.*, 2008], whereas T2 is higher than the 5 m contour along the western coast of Cheduba Island (see Figures 10 and 11). (b) The elevation difference between the modern and uplifted beach berm implies <1 m of land-level change from the latest tectonic event to present. The U-Th ages of uplifted corals beneath the modern oyster reef suggest that the event occurred after the 8th century. Black dashed line shows the approximate topography from our field observations. Blue dot is the top of the modern beach berm on T1.

block. A radiocarbon analysis of one of these oysters yields a mid-15th century to early 17th century age range (Table 1, TY-140). Thus, we conclude that the net uplift during and since the 1762 earthquake is no more than about 7–7.5 m. However, since these oysters grew on the T1b surface, the actual amount of uplift during the 1762 event in this area may be much smaller and may correspond to the elevation of T1a's shoreline angle, which we did not measure in the field.

4.2.6. Summary of Cheduba Island

[72] Our results indicate that, like Ramree Island, Cheduba Island tilted northeastward during the 1762 earthquake. The greatest uplift (3.5–4.5 m) occurred along the southwestern coast. Uplift decreased northeastward to less than 1 m at the northeastern corner of the island.

[73] As on Ramree Island, the patterns of uplift on Cheduba Island are consistent with the broad topography of the island and offshore bathymetry. This similarity implies that the 1762 pattern reflects much longer term neotectonic patterns of deformation.

5. Discussion

[74] Because our coastal survey was conducted ~250 years after the 1762 earthquake, the coastal emergence we documented reflects the coseismic uplift plus later deformation and changes in sea level. Therefore, in the following section, we first deconvolve the 1762 coseismic uplift from vertical motions reasonably ascribed to recent global sea level change and interseismic deformations. We later discuss the 1762 net-uplift pattern and compare it to the other well-documented subduction zone earthquakes. We then consider a variety of structural configurations to arrive at the most plausible fault-rupture model of the 1762 earthquake. Finally, we discuss the implications of our findings upon estimation of the earthquake magnitude, as well as nominal recurrence intervals for events like the great Arakan earthquake.

5.1. Recovering Coseismic Uplift From the Emergence Measurements

[75] Displacement of sea level indicators above or below their modern analogues may result from several different processes, not all of which are tectonic. In addition to tectonic causes such as coseismic and postseismic uplift, interseismic strain accumulation, or deformation associated with later, minor earthquakes, changes in sea level itself may also contribute. Figure 16 illustrates these plausible components to emergence measurements. Below, we attempt to untangle these contributions to our uplift measurements, so that we can understand their influences and the source parameters of the 1762 earthquake.

5.1.1. Nontectonic Water-Level Change

[76] The land-level change (Uz) that we observed along the western Myanmar coast is affected by both tectonic deformation (Ut) and nontectonic water-level change through time (S^*T). The following equations describe simply their relationships to the observed land-level change:

$$Uz = Ut + S * T \tag{1}$$

$$Ut = \Delta Z + I * T. \tag{2}$$

[77] In the latter equation, ΔZ represents the combination of coseismic and postseismic deformations. We do not separate them here, because they are difficult to separate using just our post-earthquake field measurements. Interseismic deformation (I) and sea level change (S) both accumulate with time (T).

[78] Since sea level rise varies with location [e.g., *Llovel et al.*, 2009], ideally, we would use the appropriate curve for the west coast of Myanmar. Unfortunately, such a local curve is unavailable, so we must use the estimated global average to eliminate the contribution of sea level rise to our measurements. Recent studies show that average global sea level has risen about 25 cm since the mid-19th century

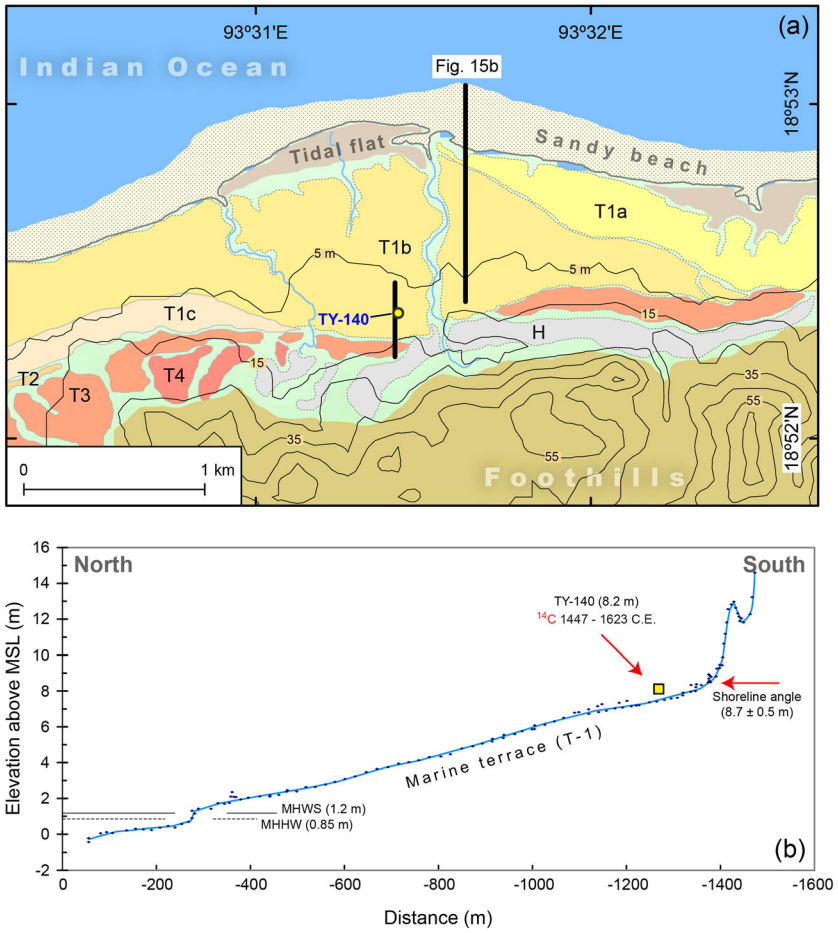

Figure 15. The age of the marine terrace in the northern part of Cheduba Island appears to suggest large uplift during the 1762 earthquake. (a) Based on the analysis of high-resolution satellite images, we separated the lowest marine terrace T1 into three subterraces (T1a, T1b, and T1c). However, the terrace risers are not clearly identifiable in the field, perhaps due to the recent agricultural disturbance. (b) A topographic profile of the area. The age of uplifted oyster fossils and preserved uplifted shoreline angle of T1 suggests ~7–7.5 m of land-level change after the 15th to 17th century.

[*Jevrejeva et al.*, 2008; *Church and White*, 2011]. If this globally averaged rise in sea level is representative of sea level change along the coast of Myanmar, then our comparisons of elevated 18th century sea level indicators with their modern counterparts would underestimate uplift by at least 25 cm. This might explain, for example, the difference between our measurement of 3.4 m at the southwestern corner of Cheduba Island and Captain Halsted's measurement of ~3.6 m [*Halsted*, 1841]. It might also partially explain why we measured 5–5.5 m of uplift on the central southwestern coast of Ramree Island, whereas Mallet reported ~6.1 m uplift in the mid-19th century [*Mallet*, 1878].

[79] Figure 17 shows net-uplift values after removal of the effect of globally averaged sea level rise. This correction reduces the differences between our measurements (the blue dots) and the observations that were made in the 19th century (the green squares). The fact that our 21st century measurements are so similar to the 19th century measurements implies that interseismic subsidence related to locking of the underlying megathrust between the mid-19th century and now is within the error of the measurements. Let us now take a closer look at this likely component to the difference between our measured sea level markers and their modern analogues.

5.1.2. Interseismic Deformation

[80] Measurements along the central to southern southwestern coast of Cheduba Island demonstrate the inability of our measurements to resolve interseismic vertical deformations. Along this part of the coast, *Halsted* [1841] measured uplifts of ~3.6–3.9 m based on the elevation of the terraces. However, he did not mention the reference level of his measurement in the original report. We assume that he referred his measurements to MSL but have to assign an uncertainty equal to the tidal range of ± 1.4 m in this area. The microatolls we surveyed near the village of Ka-I suggest a net uplift of 3.7 ± 0.2 m, after the sea level rise correction. As a result, the land-level change produced by interseismic deformation through the past 170 years is 0.05 ± 1.6 m. This yields a range of interseismic deformation rates (I) that is not very informative—somewhere between subsidence at 9 mm/yr and emergence at 10 mm/yr.

[81] Modern observations suggest that the coastline has subsided between earthquakes. *Shishikura et al.* [2009] noted that a comparison of old topographic maps with

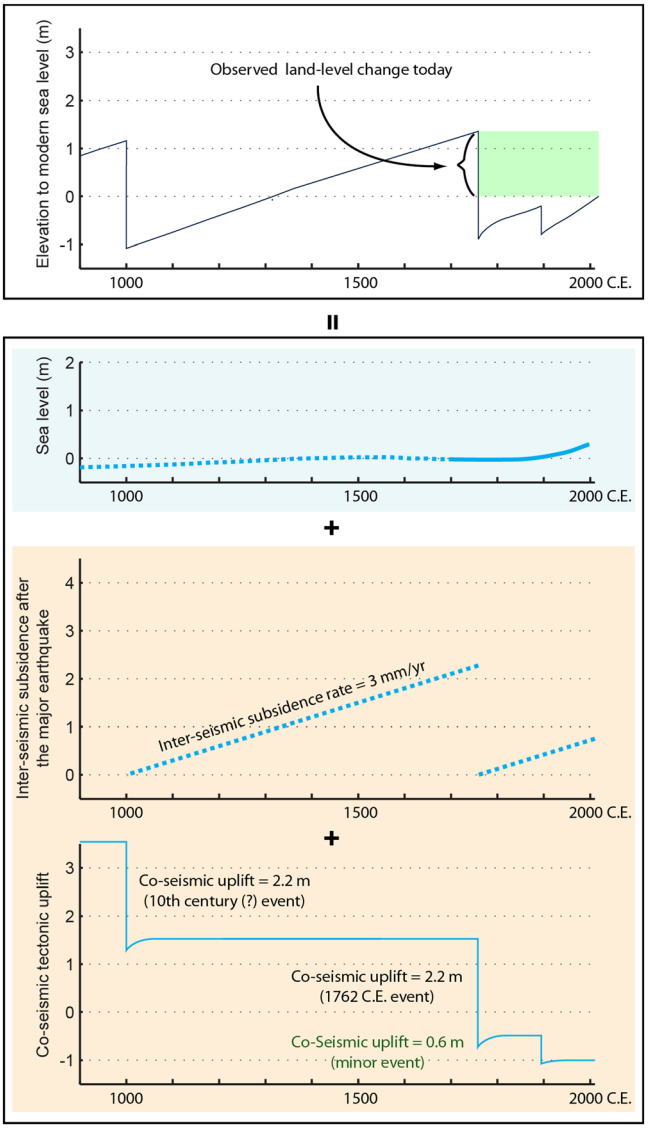

Figure 16. A cartoon that shows the contributions of various processes to sea level history of the past several hundred years. The green shaded area indicates why the net land-level change that we surveyed may well be different than the uplift of 1762.

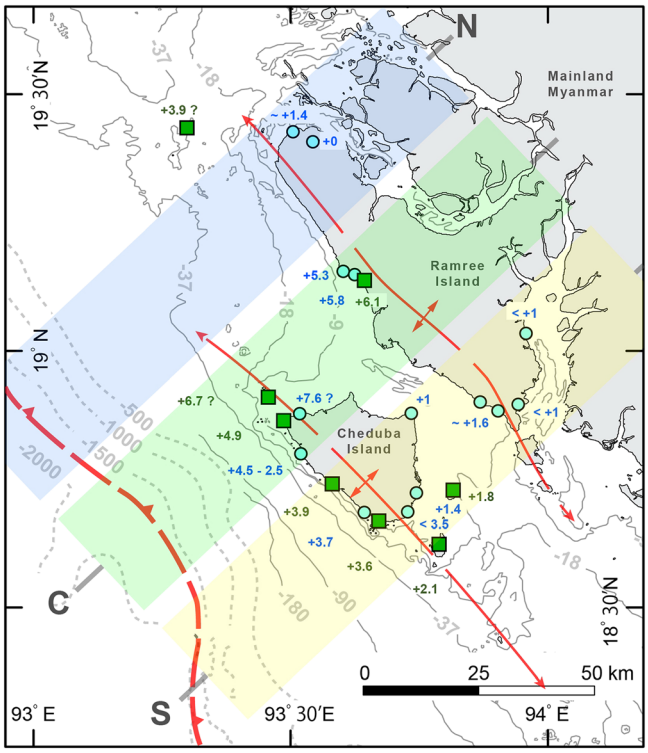

Figure 17. A compilation of measurements of 1762 uplift values, from our surveys (circles) and 19th century documents (squares). The pattern of 1762 uplift suggests that Cheduba and Ramree Islands uplifted as separate anticlinal welts. This coseismic pattern mimics the anticlinal forms visible in the onshore and offshore topography. Hence, we suggest that the 1762 earthquake was associated with incremental uplift of two doubly plunging anticlines above the megathrust. Colored bars indicate the bands from which data were taken to create the three uplift profiles of Figure 18.

current topography implies subsidence of Cheduba Island. The concave upward morphology of the upper surfaces of coral microatolls at the southern tip of Cheduba Island indicates that the coast there was subsiding in the decades prior to uplift of the microatolls in 1762. Thus, we can constrain the interseismic rate (I) to between -9 and 0 mm/yr along the southern coast of Cheduba Island.

[82] In fact, our interpretation of interseismic subsidence roughly coincides with the prediction from a simple back slip elastic deformation model. By assuming a fully locked 16° dipping megathrust above 30 km in depth, the 23 mm/yr plate motion between the Indian and the Burma plates reveals a 5 to 3 mm/yr subsidence rate from the southwestern Cheduba to the southwestern Ramree coasts. Unfortunately, because the interseismic deformations vary not only as a function of the distance from the trench but also as a function of the fault coupling ratio, these estimations can be only treated as the maximum subsidence rate above the megathrust. Nevertheless, this maximum constraint shows that the deficit between the true coseismic uplifts and our net-uplift observation is likely smaller than 1 m, assuming a maximum 4 mm/yr average subsidence rate in this region.

5.1.3. Possible Later Uplift Events

[83] We now consider the possibility that deformation related to other earthquakes contributes to our measurements. Historical records affirm that the 1762 earthquake was the largest earthquake along the northern Sunda megathrust in the past few hundred years. Nonetheless, several other strong earthquakes did occur in the 19th century [*Oldham*, 1883]. The most plausible candidates for having produced additional deformation in the region are earthquakes in 1848 and 1858. Northern Ramree Island experienced strong shaking during these events. Historical records, however, contain no hint that Cheduba and Ramree Islands rose during these events. For example, Mallet made no mention of any recent coastal uplift seen during his visit to the central southwestern Ramree coast in 1877 other than the 1762 event. Instead, he reported that the coastline of Round Island in Captain Halsted's map was very similar to the coastline geometry at the time of his visit. Our surveys of central

Table 3. Net uplift in Ramree and Cheduba Islands Inferred From Sea Level Indicators

Name	Location		Uplift Feature	Elevation (m)		Reference Level	Elevation (m)		Land-Level Change (m)		Calibrated Net Uplift (m)[a]		Survey Method[b]	Remark
	Latitude	Longitude												
Northern Ramree Island														
E-KPU	19.41	93.53	Coral, microatolls	1.3	±0.2	MLLW	−0.8	±0.2	2.2	±0.3	2.4	±0.3	T.S.	Mid-Holocene
KPU15_O	19.43	93.51	Uplift Oyster	2.2	±0.1	Living oysters	1.2	±0.1	1.0	±0.2	1.2	±0.2	T.S.	
KPU15_N	19.43	93.51	Tidal notch	1.5	±0.1	Active tidal-notch	0.1	±0.2	1.4	±0.3	1.7	±0.3	T.S.	
Central Ramree Island														
Mallet (1878)	19.15	93.6	Raised beach	6.1	–	MSL?	–	±1.3	–	–	6.1	±1.3	–	*Mallet*, 1878
ZC16_C	19.16	93.60	Coral, microatolls	4.2	±0.1	MLLW	−0.8	±0.2	5.0	±0.2	5.3	±0.2	T.S.	Confirmed by U-Th date
ZC16_O	19.16	93.60	Oyster fossils	5.7	±0.1	MHHW	0.9	±0.3	4.8	±0.3	5.1	±0.3	T.S.	
ZC16-SA	19.16	93.60	Shoreline angle	5.8	±0.1	Shoreline angle	0.9	±0.4	5.0	±0.4	5.2	±0.4	T.S.	
ZC04	19.15	93.63	Uplifted platform	5.5	±0.1	Shoreline angle	–	–	5.5	±0.1	5.8	±0.1	L.R.	Min. Constrain
Southern Ramree Island														
KYM	18.90	93.96	Shoreline angle	4.0	±1.0	Shoreline angle	–	–	4.0	±0.1	4.3	±0.1	E.L.	Mid-Holocene
TKN_N	18.89	93.89	Shoreline angle	2.7	±0.1	MHWS	1.3	+ 1.0	1.4	- 1.0	1.6	- 1.0	T.S.	
TKN_N	18.89	93.89	Surge notches	2.7	±0.4	MHWS	1.3	+ 1.0	1.4	- 1.1	1.7	- 1.1	T.S.	
TKC	18.89	93.90	Shoreline angle	2.9	±0.1	Shoreline angle	1.3	±0.1	1.6	±0.1	1.9	±0.1	T.S.	
TKS	18.88	93.91	Shoreline angle	2.6	±0.1	Shoreline angle	1.4	±0.1	1.2	±0.1	1.5	±0.1	T.S.	
WTK	18.90	93.87	Shoreline angle	2.2	±0.4	MHWS	1.3	+ 1.0	0.9	- 1.1	1.1	- 1.1	L.R.	
WTK	18.90	93.88	Shoreline angle	2.9	±0.4	MHWS	1.3	+ 1.0	1.6	- 1.1	1.8	- 1.1	L.R.	
Eastern Ramree Island														
ERM	19.03	93.96	Tidal notch	4.2	±0.5	MSL	0.0	±1.0	4.2	±1.1	4.5	±1.1	R.M.	Mid-Holocene?
ERM	19.03	93.96	Shoreline angle	2.1	±0.5	MHWS	1.4	+ 1.0	0.7	- 1.1	1.0	- 1.1	R.M.	
Man-Aung, Cheduba Island														
MA_C	18.88	93.72	Coral fossils	−0.6	±0.1	MLLW	−0.9	±0.2	0.3	±0.2	0.5	±0.2	L.R.	Min. net uplift since 600 C.E.
MA_B	18.88	93.72	Uplift beach berm			Beach berm			0.8	±0.2	1.1	±0.2	L.R.	
MA_T	18.88	93.74	Uplift platform	2.1	±0.4	MHWS	1.3	–	0.8	±0.4	1.1	±0.4	L.R.	Min. Constrain
Ka-Ma, Cheduba Island														
NW_Che	18.87	93.5	Elevated terrace	4.8	–	MSL?	–	±1.3	–	–	4.8	±1.3	–	*Halsted*, 1841
KM	18.81	93.52	Coral, microatolls	3.4	±0.1	MLLW	−0.8	±0.2	4.2	±0.2	4.5	±0.2	T.S.	Max. Constrain
KM	18.81	93.52	Shoreline angle	3.4	±0.5	MHWS	1.2	+ 1.0	2.2	- 1.1	2.5	- 1.1	T.S.	Min. Constrain
Ka-I, Cheduba Island														
C_Che	18.75	93.6	Elevated terrace?	3.9	–	MSL?	–	±1.3	–	–	3.9	±1.3	–	*Halsted*, 1841
S_Che	18.67	93.7	Elevated terrace	3.6	–	MSL?	–	±1.3	–	–	3.6	±1.3	–	*Halsted*, 1841
KI	18.68	93.64	Coral, microatoll	2.4	±0.1	MLLW	−1.1	±0.2	3.4	±0.2	3.7	±0.2	T.S.	Confirmed by U-Th date
Eastern Cheduba Island														
KK	18.72	93.74	Shoreline angle	2.3	±0.1	MHWS	1.2	+ 1.0	1.1	- 1.0	1.4	- 1.0	T.S.	Min. Constrain
SC	18.70	93.73	Shoreline angle	4.5	±0.5	MHWS	1.2	+ 1.0	3.3	- 1.1	3.5	- 1.1	REF.	Max. Constrain
Northwestern Cheduba Island														
NW Reef	18.93	93.45	Elevated rocks?	6.7	–	MSL?	–	±1.3	–	–	6.7	±1.3	–	*Halsted*, 1841 (unconfirmed)
DY	18.88	93.53	Oysters	8.2	±0.1	MHHW	0.85	±0.3	7.4	±0.3	7.6	±0.3	T.S.	Max. Constrain
	18.88	93.53	Shoreline angle	8.7	±0.5	MHWS	1.2	+ 1.0	7.5	- 1.1	7.8	- 1.1	T.S.	Max. Constrain
Other Islands														
FLAT	18.62	93.77	Elevated terrace	2.1	–	Sea level	0	±1.4	–	–	2.1	±1.4	–	*Halsted*, 1841
Round	18.73	93.81	Shell taxa	1.8		High tide	–	±0.5	–	–	1.8	±0.5	–	*Mallet*, 1878

[a]Calibrated net uplift (m) = Land-level change − Sea level change from the 19th to 21st century. The amount of sea level change is from Jevrejeva et al. [2008].
[b]T.S. = Surveyed by total station; L.R. = surveyed by laser range finder; R.M. = remote measurement; E.L. = surveyed by eye-leveling; REF. = data from published references.

southwestern Ramree Island and southwestern Cheduba also show that the last emergence occurred in the 18th century. Since we lack evidence of post-1762 uplift along these coasts, and since strong shaking reports are limited to northern Ramree Island, we believe that significant coastal uplift of the entire coast did not occur during the earthquakes of the mid-19th century. Nonetheless, lesser local uplift may have occurred but gone unreported along, for example, the northern Ramree Island.

5.2. The Uplift Pattern of the 1762 Earthquake

[84] Despite these minor ambiguities, our survey results still improve significantly our knowledge of deformations associated with the 1762 earthquake. The density of observations on Cheduba and Ramree Islands, for example, is now much greater (Figure 17 and Table 3). Our U-Th results also provide age constraints that demonstrate uplift in 1762 C.E. along both the western coast of Ramree Island and the entire coast of Cheduba. Our observations, together with the historical accounts, provide a general net-deformation pattern for the 1762 earthquake.

[85] In general, as previous studies have suggested, the largest uplifts of 1762 were 3–4 m along the western coast of Cheduba Island. Elsewhere along the coast of Cheduba, 1762 uplift ranges from ~2 to ~1 m. Uplift is smallest (<1 m) at the northeastern corner of the island.

[86] Along the western coast of Ramree Island, the net-deformation pattern is more complicated. The vertical deformations decrease not only northeastward, moving away from the trench, but also parallel to the trench, from a high of about 6 m along the central western Ramree coast. It is noteworthy that even the lesser amounts of uplift along the western coast of Ramree island (~1–2 m) are higher than uplift closer to the trench, on the northeastern tips of Cheduba Island. Taken together, the deformation of Ramree and Cheduba Islands is double peaked, with highs along the trenchward coasts of both islands (Figure 18).

5.3. The Significance of the Upper Plate Structures

[87] The double-hump uplift pattern of 1762 coincides with the regional antiformal shape of Cheduba and Ramree Islands and the associated bathymetry. These two trench-parallel active antiforms are apparent in the topography and bathymetry in Figure 17. The two red dashed lines there represent the crests of the antiforms inferred from the shallow water bathymetry (Figure 1). The fact that the southwestern flanks of the anticlines are topographically steeper than the northeastern flanks implies an asymmetric fold geometry.

[88] Although the locations of the greatest 1762 uplift are not exactly coincident with the anticlinal crests, the similarity between the pattern of uplift in 1762 and the form of the anticlines leads us to hypothesize that the upper plate secondary structures associated with the antiforms ruptured during the 1762 event. Such failure of multiple splay faults during a single earthquake is not unknown; multiple failures occurred during other large thrust-fault earthquakes, such as the 1964 Alaskan earthquake [*Plafker*, 1965] and the 2008 Wenchuan earthquake [*Xu et al.*, 2009].

[89] The evidence of splay faulting is quite clear across the central profile. The magnitude and gradient across the central southwestern Ramree coast is unlike any documented

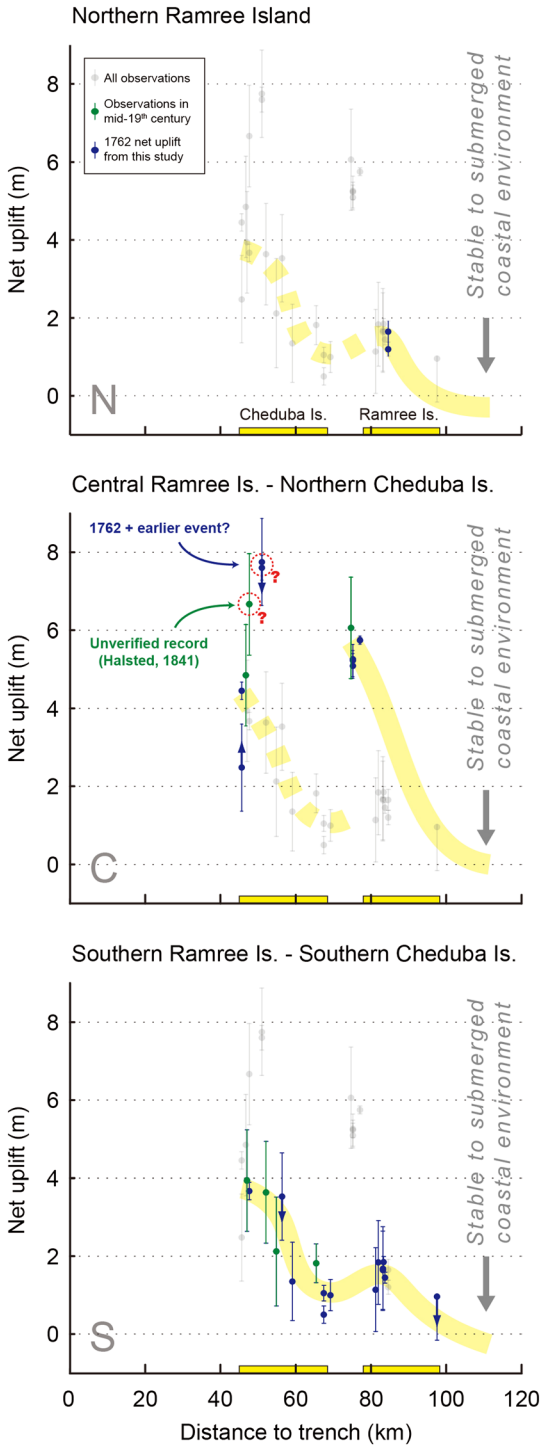

Figure 18. Three profiles of net post-1762 uplift drawn perpendicular to the megathrust. All the data from the islands appear in each profile as gray line with their uncertainties. Measurements unique to each profile appear as dark blue (modern) and green (historical) dots. Thick yellow lines show inferred uplift pattern across each profile. The highest uplifts appear along the central profile (C). This suggests either highest fault slip on the megathrust or a change in fault geometry along this profile. Red dashed circles with question marks are measurements that we suspect to be overestimated.

pure megathrust rupture (Figure 19, right). Magnitudes and gradients this steep did, however, occur during the 1960 Chilean and the 1964 Alaskan earthquakes (Figure 19, left). Previous studies imply that both of these earthquakes involved failure of large splay faults [e.g., *Plafker*, 1972]. In the case of the Alaskan earthquake, two splay faults clearly ruptured the surface on each side of an offshore island. The similarity between the 1762 uplift pattern and the 1964 Alaskan earthquake pattern strongly suggests that splay faulting was involved during the 1762 Arakan earthquake, and both faults beneath Ramree and Cheduba Islands moved during this event.

[90] However, rupture on the splay faults may not explain all the deformation of the 1762 event. The magnitude and gradient of vertical deformation across the southern profile are not as sharp as they are across the central profile. The

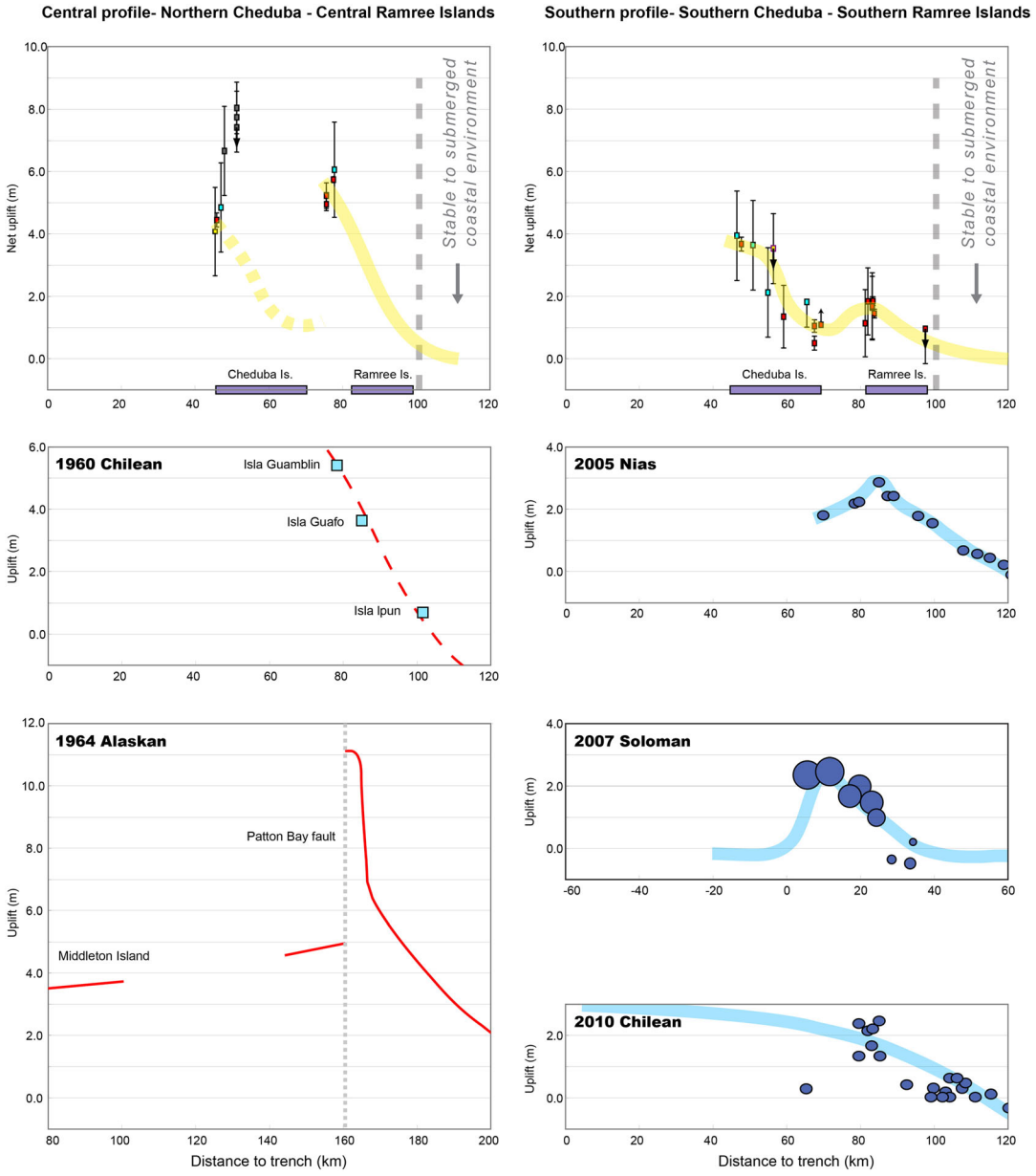

Figure 19. A comparison of trench-perpendicular uplift patterns of several well-documented megathrust earthquakes and the 1762 event supports the hypothesis that the 1762 pattern resulted in part from slip on splay faults beneath the islands. The steep gradients along the central profile are similar to those for earthquakes in which splay faults ruptured. The three deformation profiles in the lower right panels have low gradients and are believed to have resulted from simple slip on the megathrust. The two deformation profiles in the lower left panels exhibit large uplifts and steep gradients caused by slip on underlying splay faults. The 1960 Chilean and 1964 Alaskan uplift patterns are from *Plafker* [1972]; uplift pattern of the Nias earthquake of 2005 is from *Briggs et al*. [2006]; uplift pattern of the Solomon earthquake of 2007 is from *Taylor et al*. [2008], and the 2010 Chilean earthquake's land-level change distribution is from *Farías et al*. [2010].

broad uplift pattern across the southern profile is similar to that expected of a pure megathrust rupture. Thus, the rapid southward diminishment of slip on one of the splay faults may imply slip on the megathrust alone beneath the southern profile. Moreover, the two antiforms manifested by the two islands are ~100 km long, only a fraction of the 500 km length of reported coastal deformation during the 1762 earthquake [e.g., *Oldham*, 1883; *Cummins*, 2007]. Therefore, we believe that the Arakan earthquake of 1762 resulted from rupture of both the megathrust and major splay faults.

5.4. The Source of the 1762 Earthquake

[91] We hypothesize that slip on the faults that produced the 1762 earthquake should also be able to produce the long-term deformation of Ramree and Cheduba Islands. The subsurface structures beneath the islands are poorly known, so the best approach to inferring their geometry is to test a variety of geometries to explore which are the most plausible for generating both the 1762 uplift pattern and the islands' topography.

[92] We propose three structural geometries: a simple megathrust model, a megathrust model with a ramp, and a megathrust model with two splay faults (Figure 20). We fixed the dip angle of the northern Sunda megathrust to be 16° in the simple megathrust model and in the splay-fault model. In the ramp model, we added a 30° fault ramp along a 10° dipping megathrust. In the splay-fault model, we added two splay faults beneath Cheduba and Ramree Islands, with the splay faults cropping out several kilometers southwest of the southwestern coasts of the islands. We assume that the dip of each of the splay faults is 45°, so that these upper plate faults would be able to connect to the megathrust beneath the eastern limb of these antiforms. We also assume that coseismic fault slip on the splay faults is partitioned from the megathrust; hence, the more slip on the splay faults, the less slip would propagate updip along the megathrust.

[93] All three models are capable of producing a double-hump uplift pattern similar to that measured along our southern profile (Figure 20). The greatest depth of slip on the fault plane is no deeper than 30–35 km in these models, as is typical for the seismic megathrust ruptures. However, the long-term uplift patterns vary significantly in these models due to the differential uplift rates above the fault produced by different fault geometries [e.g., *Hubert-Ferrari et al.*, 2007]. We found that only the splay-fault model is able to produce the long-term deformation pattern of the two antiforms. On the contrary, the simple megathrust model produces a uniform vertical deformation pattern relative to the footwall block, while the megathrust with ramp model generates a broad fault-bend fold above the ramp area. This result further supports our idea that the splay-fault model is the most appropriate source geometry for the 1762-type earthquake along the northern Sunda megathrust belt.

[94] In order to fit the 1762 net-uplift patterns using the splay-fault model, the required total slip on the megathrust and the splay faults ranges from 9 to 16 m (Figure 21). Along the southern profile, our solution shows that the 45° blind splay fault beneath Ramree Island absorbs ~1.5 m slip from the megathrust, and the total slip on the megathrust is ~9 m above a depth of 32 km. Farther west, more than 65% of slip (>5 m) partitioned from the megathrust to the other splay fault beneath Cheduba Island, creating nearly 4 m of uplift along its southwestern coast. The deformation pattern across northern Ramree Island may be also explained by a similar slip pattern.

[95] Maximum fault slip occurred beneath the central profile, from northern Cheduba Island to central Ramree Island. Our solution suggests slip of ~16 m beneath this profile. Nearly 55% of slip (~8 m) partitioned to the splay fault

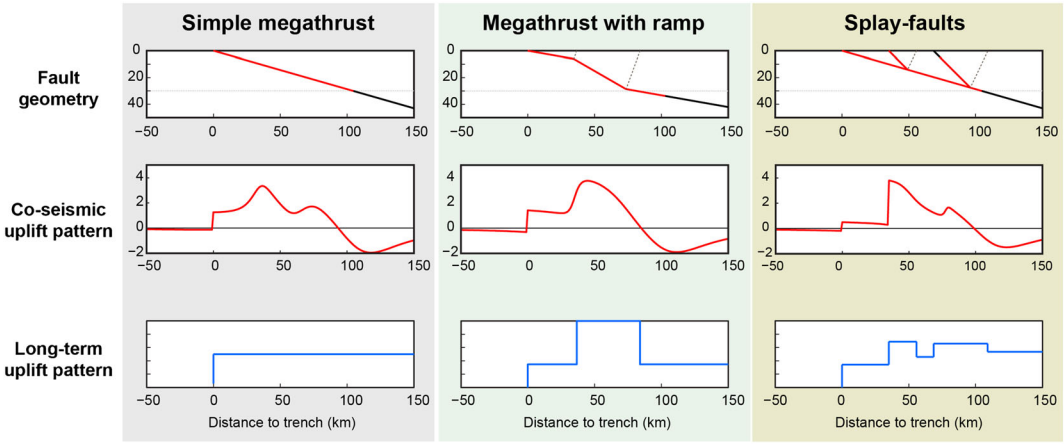

Figure 20. A cartoon diagram that shows the coseismic uplift pattern and long-term deformation pattern produced by three different scenario fault ruptures. Red lines in the upper panels show the part of the fault or faults that slip during an earthquake. We apply the uniform slip constraint on each section of the fault in the ramped megathrust and the splay-fault model, and the nonuniform slip to the simple megathrust model. The coseismic uplift patterns of such an earthquake appear in the central row. All of the three geometries appear to be able to produce similar coseismic deformation patterns. However, the long-term uplift patterns related to these geometries, shown as the light blue lines in the lower panels, are different. Only the megathrust model with splay faults is capable of producing the double hump topography of Cheduba and Ramree Islands.

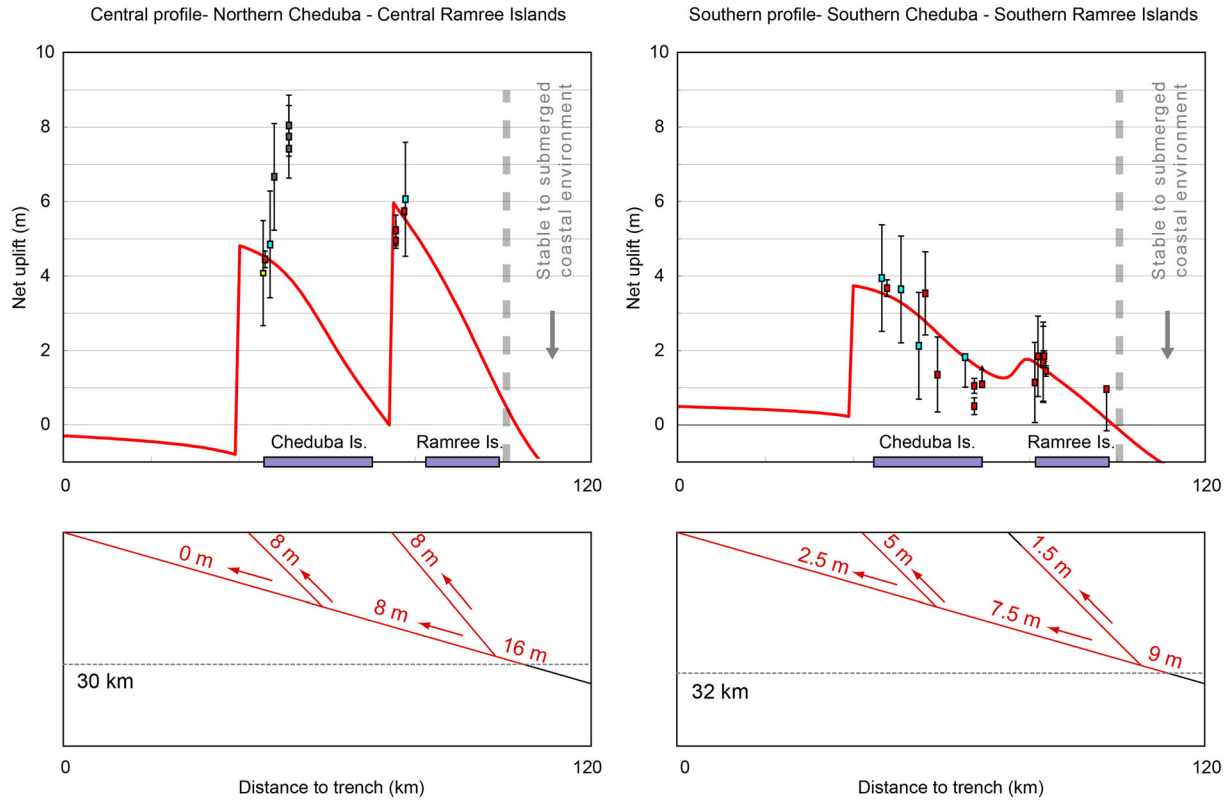

Figure 21. Plausible 1762 fault slip patterns beneath the central and southern profiles across Cheduba and Ramree Islands. The red lines in the upper panels show the uplift patterns. The lower panels show the fault geometries and amount of slip on the megathrust and splay faults for each model. The grey-dashed lines indicate the maximum depth of fault slip.

beneath Ramree Island, if the fault dips 50° beneath the island. Under Cheduba Island, the frontal splay fault may have taken all the rest of slip from the megathrust (~8 m), in order to fit the 4 m uplift of the northern southwestern Cheduba coast.

[96] From the modeled fault slip on the megathrust during the 1762 event, we are able to calculate the magnitude of the earthquake. Since the rupture area on the splay faults is much smaller than that on the megathrust itself, we chose to calculate the moment magnitude using only the rupture area on the megathrust. Our model suggests that the megathrust slips 7.5 m or more between the depth of 14 and 32 km, which is more than 50% of the fault's seismogenic width. Above the depth of 14 km, the slip on the megathrust is minimal in our model. Therefore, the rupture width is ~60 km along the megathrust, with an average slip of 7.5 m. We assumed the fault length to be 500 km based on the historical land-level change records from Foul Island to Chittagong, comparable to the length used by *Cummins* [2007]. Together, these parameters suggest the magnitude of 1762 earthquake is M_w 8.5.

[97] The estimated M_w 8.5 of 1762 earthquake is about 2.8 times smaller than the M_w 8.8 estimated by *Cummins* [2007]. The principle reason is that in our model, the slip is partitioned between the megathrust and the splay faults. As a result, our modeled fault width and the coseismic slip are smaller. However, it is unlikely that such a splay fault geometry would remain the same along the entire 500 km length of the megathrust. Furthermore, we did not include the rupture of the splay faults or the slip on the shallow part of the megathrust in our calculation. Thus, our estimate provides a plausible lower bound for the magnitude of the 1762 earthquake.

5.5. Earthquake Recurrence Intervals

[98] Both paleoseismological and historical evidence for repeating great earthquakes along the northern Sunda megathrust is scant. Earthquake stories told by local villagers and geomorphic observations from previous studies suggest that events similar to the 1762 earthquake recur every several centuries to every millennium or so [e.g., *Halsted*, 1841; *Shishikura et al.*, 2009]. To estimate a plausible range for an average recurrence interval, we used the following equation to calculate the seismic interval (ΔT) from the long-term uplift rate (R), the interseismic deformation rate (I), and the amount of coseismic uplift (ΔZ) based on the characteristic slip model:

$$\Delta Z/\Delta T + I = R. \tag{3}$$

[99] In equation (3), we assumed that the long-term deformation is the sum of the interseismic deformation and the coseismic plus postseismic deformations. Therefore, if the uplift event occurs regularly, the relationship can be written in the form of equation (3), in which ΔT represents the recurrence interval. Since the actual coseismic deformation (ΔZ) is poorly constrained from geomorphic studies after the earthquake, we use the observed net uplift (Ut) in equation (2) to replace ΔZ by combining equations (2) and (3), i.e.,

$$(Ut - I * T)/\Delta T + I = R. \quad (4)$$

[100] Hence, the recurrence interval (ΔT) changes as the function of the interseismic deformation rate (I) as we rearrange equation (4) to equation (5), i.e.,

$$\Delta T = (Ut - I * T)/(R - I) \quad (5)$$

[101] At the southwestern corner of Cheduba Island, the long-term uplift rate (R) that we estimated from coral fossils found in higher elevations is between ~3.5 and ~5.2 mm/yr. The observed net uplift (Ut) from the 1762 earthquake to present is 3.7 m, and the estimated interseismic uplift rate (I) ranges from −9 to 0 mm/yr, more likely between −5 and −3 mm/yr as predicted in the back slip elastic model. As a result, the ΔT ranges from 400 to 700 years if the long-term uplift rate (R) is about 5 mm/yr. If the long-term uplift rate (R) is slower, such as 3.5 mm/yr, the corresponding recurrence interval (ΔT) would change to between about 450 and about 1000 years (Figure 22). If we apply the −5 to −3 mm/yr interseismic uplift rate predicted from the back slip model to this diagram, we can further narrow down the 1762-type recurrence interval to ~500 to ~700 years under the same conditions.

[102] Such range of recurrence interval is very close to the estimations from our elastic deformation model, in which we suggest that the maximum fault slip is about 16 m beneath Ramree Island. By dividing 16 m to the 23 mm/yr plate motion between the Indian and the Burma plates, we estimated the recurrence interval to be ~700 years. The similarity between these two independent estimations again supports our splay-fault model, in which the major deformation results from the activity of upper plate structures, rather than the megathrust itself.

[103] This 500–700 years interval is similar, but shorter than the recurrence intervals (~900 years) estimated by previous studies [e.g., *Than Tin Aung et al.*, 2008; *Shishikura et al.*, 2009]. The earlier estimations heavily rely on the ages of uplifted terraces; thus, any events that did not produce the emergence of marine terraces may be ignored in their studies. Our preliminary U-Th analyses of uplifted corals in southwestern Cheduba coast show that such undocumented events may exist in the past 1000 years. These undocumented events may result from minor slips on the upper plate secondary structures or pure failure of the megathrust that does not produce any long-term deformation. The occurrence of such events may result in shorter earthquake recurrence intervals than what we estimated from the characteristic slip model. Thus, more detailed field investigations are necessary along the western coast of Myanmar to understand the detailed deformation history in the past several thousand years.

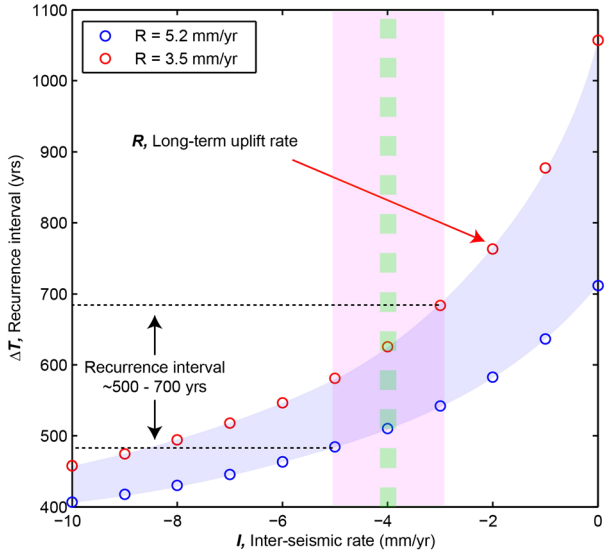

Figure 22. Range of nominal recurrence intervals for 1762-like earthquakes, based on the relationships between the long-term uplift rate and the interseismic subsidence rate at the southwestern corner of Cheduba Island (Ka-I area). We suggest the nominal recurrence interval ranges from ~400 to ~1000 years. Blue-shadowed area shows the range of the long-term uplift rate from uplifted corals in Ka-I area, and green dashed line depicts the average interseismic subsidence rate from the elastic deformation model. The pink-colored bar shows the range of the subsidence rates from the model. If the modeled interseismic subsidence rate represents the actual subsidence rate between two seismic events, the recurrence interval of 1762-like events would be ~500 to ~700 years.

6. Summary and Conclusions

[104] From field observations and age analysis of uplifted coral and oyster fossils, we have obtained a detailed data set of coastal uplift amount of Ramree and Cheduba Islands during the 1762 Arakan earthquake. Up to 6 m of uplift occurred at the central western Ramree coast during the earthquake, as recorded by observations in the 19th century. Our remote sensing study and field investigations also suggest that the entire Ramree Island has been affected by an eastward tilting during the Holocene epoch. This regional tilting coincides with the net-uplift pattern of the 1762 earthquake, during which only western Ramree Island uplifted significantly.

[105] Results of our field surveys enabled us to determine the net-uplift pattern of the 1762 Arakan earthquake along the southern part of the northern Sunda megathrust. A net-uplift profile perpendicular to the trench from the western Cheduba coast to eastern Ramree Island shows the net-uplift amount decreases from ~4 m in the west to nearly 0 m in the east. A secondary net-uplift high is present at central western Ramree Island. This double-hump uplift pattern coincides with the long-term uplift patterns of Ramree and Cheduba Islands and is difficult to explain by pure elastic deformations of the megathrust. Thus, we propose that upper plate splay faults play important roles in the 1762 earthquake.

[106] By fitting the coastal net-uplift data with the simple megathrust-splay faults model, we estimate the total slip on the megathrust-splay fault system to have been about 9–16 m beneath Cheduba and Ramree Islands. This modeling result also indicates that the 1762 earthquake had a moment magnitude of about 8.5. This estimation is likely a minimum, because we ignored the contributions from slip along the shallow megathrust and from slip on the splay faults.

[107] Our first-order estimation shows that the recurrence interval of events similar to the 1762 earthquake ranges from ~400 years to less than 1000 years and is most likely between 500 and 700 years, along the northern Sunda megathrust. Since the last large earthquake occurred nearly 250 years ago, detailed paleoseismological studies are urgently needed in order to understand the earthquake history and future earthquake hazards along the northern Sunda megathrust.

[108] **Acknowledgments.** We have benefited greatly from discussions with Win Swe, J.-P. Avouac, and M. Shishikura. We also appreciate the generous support of the Immediate Past President of the Myanmar Engineering Society (MES), U Than Myint, and the assistance from members of the Myanmar Geosciences Society (MGS), the Department of Meteorology and Hydrology (DMH) of Myanmar, and Thingazar Travels & Tours Company. The comments and suggestions of R. Bilham and an anonymous reviewer significantly improved this manuscript. This research was supported by the Earth Observatory of Singapore (EOS) and by the National Science Council (NSC) of Taiwan (NSC 99-2116-M-002-009, 100-2116-M-002-005, and 101-2116-M-002-013 to J.B.H.S.). U-Th dating at the HISPEC was supported by NSC grant 100-2116-M-002-009 to C.-C.S. This is Earth Observatory of Singapore contribution number 46 and Caltech Tectonics Observatory contribution number 218.

References

Agnew, D. C. (1997), NLOADF: A program for computing ocean-tide loading, *J. Geophys. Res.*, *102*, 5109–5110.

Amante, C., and B. W. Eakins (2009), ETOPO1 1 Arc-Minute Global Relief Model: Procedures, Data Sources and Analysis, NOAA Technical Memorandum NESDIS NGDC-24, 19 pp.

Awata, Y., S. Toda, H. Kaneda, T. Azuma, H. Horikawa, M. Shishikura, and T. Echigo (2008), Coastal deformation associated with the 2007 Noto Hanto earthquake, central Japan, estimated from uplifted and subsided intertidal organisms, *Earth Planets Space*, *60*, 1059–1062.

Beaman R, P. Larcombe, and R. M. Carter (1994), New evidence for the Holocene sea-level high from the inner shelf, central Great Barrier Reef, Australia, *J. Sediment. Res., Sect. A*, *64*, 881–885.

Briggs, R. W., et al. (2006), Deformation and slip along the Sunda megathrust in the great 2005 Nias-Simeulue earthquake, *Science*, *311*, 1897–1901.

Briggs, R. W., et al. (2008), Persistent elastic behavior above a megathrust rupture patch: Nias island, West Sumatra, *J. Geophys. Res.*, *113*, B12406, doi:10.1029/2008JB005684.

Brunnschweiler, R. O. (1966), On the geology of the Indo-Burma ranges, *J. Geol. Soc. Aust.*, *13*, 127–194.

Chappell, J., A. Chivas, E. Wallensky, H. A. Polach, and P. Aharon (1983), Holocene palaeo-environmental changes, central to north Barrier Reef inner zone, *J. Aust. Geol. Geophys.*, *8*, 223–235.

Chen, M.-C., C. Frohlich, F. W. Taylor, G. Burr, and A. Q. van Ufford (2011), Arc segmentation and seismicity in the Solomon Islands arc, SW Pacific, *Tectonophysics*, *507*, 47–69.

Cheng, H., R. L. Edwards, J. Hoff, C. D. Gallup, D. A. Richards, and Y. Asmerom (2000), The half-life of uranium-234 and thorium-230, *Chem. Geol.*, *169*, 17–33.

Chlieh, M., *et al*. (2007), Coseismic slip and afterslip of the great (Mw 9.15) Sumatra-Andaman earthquake of 2004, *Bull. Seismol. Soc. Am.*, *97*, S152–S173.

Church, J., and N. White (2011), Sea-level rise from the late 19th to the early 21st century, *Surv. Geophys.*, *32*, 1–18.

Cummins, P. R. (2007), The potential for giant tsunamigenic earthquakes in the northern Bay of Bengal, *Nature*, *449*, 75–78.

Curray, J. R. (1991), Possible greenschist metamorphism at the base of a ~22-km sedimentary section, Bay of Bengal, *Geology*, *19*, 1097–1100.

Curray, J. R., F. J. Emmel, D. G. Moore (2003), The Bengal fan: morphology, geometry, stratigraphy, history and processes, *Mar. Pet. Geol.*, *19*, 1191–1223.

Darwin, C. (1845), Journal of Researches Into the Natural History and Geology of the Countries Visited during the Voyage of H.M.S. 'Beagle' Round the World: Under the Command of Capt. Fitzroy, 2nd ed., Corrected with Additions, John Murray, London.

Davis, A. M., J. C. Aitchison, P. G. Flood, B. S. Morton, R. G. V. Baker, and R. J. Haworth (2000), Late Holocene higher sea-level indicators from the South China coast, *Mar. Geol.*, *171*, 1–5.

DeDontney, N., and J. R. Rice (2012), Tsunami wave analysis and possibility of splay fault rupture during the 2004 Indian Ocean earthquake, *Pure Appl. Geophys.*, *169*, 1707–1735.

Farías, M., G. Vargas, A. Tassara, S. Carretier, S. Baize, D. Melnick, and K. Bataille (2010), Land-level changes produced by the Mw 8.8 2010 Chilean earthquake, *Science*, *329*, 916.

Fukao, Y. (1979), Tsunami earthquakes and subduction processes near deep-sea trenches, *J. Geophys. Res.*, *84*, 2303–2314.

Halsted, E. P. (1841), Report on the Island of Chedooba, *J. Asiatic Soc. Bengal*, *114*, New Series No. 27, 419–436.

Hopley, D. (1986), Corals and reefs as indicators of paleo-sea levels with special reference to the Great Barrier Reef, in Sea-Level Research: A Manual for the Collection and Evaluation of Data, edited by O. V. van de Plassche, GeoBooks, Norwich.

Hsieh, M. L., and R. J. Rau (2009), Late Holocene coseismic uplift on the Hua-tung coast, eastern Taiwan: Evidence from mass mortality of intertidal organisms, *Tectonophysics*, *474*, 595–609.

Hubert-Ferrari, A., J. Suppe, R. Gonzalez-Mieres, and X. Wang (2007), Mechanisms of active folding of the landscape (southern Tian Shan, China), *J. Geophys. Res.*, *112*, B03S09, doi:10.1029/2006JB004362.

Hull, A. G. (1987), A late Holocene marine terrace on the Kidnappers coast, North Island, New Zealand, *Quat. Res.*, *28*, 183–195.

Jaffey, A. H., K. F. Flynn, L. E. Glendenin, W. C. Bentley, and A. M. Essling (1971), Precision measurement of half-lives and specific activities of U-235 and U-238, *Phys. Rev.*, *4*, 1889–1906.

Jarvis, A., H. I. Reuter, A. Nelson, and E. Guevara (2008), Hole-Filled SRTM for the Globe Version 4, available from the CGIAR-CSI SRTM 90m Database, (http://srtm.csi.cgiar.org).

Jevrejeva, S., J. C. Moore, A. Grinsted, and P. L. Woodworth (2008), Recent global sea level acceleration started over 200 years ago?, *Geophys. Res. Lett.*, *35*, L08715, doi:10.1029/2008GL033611.

Kato, T. (1983), High-angle reverse faulting associated with the 1946 Nankaido earthquake, *Tectonophysics*, *96*, 31-44.

Kayanne, H., et al. (2007), Coseismic and postseismic creep in the Andaman Islands associated with the 2004 Sumatra-Andaman earthquake, *Geophys. Res. Lett.*, *34*, L01310, doi:10.1029/2006GL028200.

Kelletat, D., (1988), Zonality of modern coastal processes and sea-level indicators, *Palaeogeogr. Palaeoclimatol. Palaeoecol.*, *68*, 219–230.

Kench, P. S., S. G. Smithers, R. F. McLean, and S. L. Nichol (2009), Holocene reef growth in the Maldives: evidence of a mid-Holocene sea level highstand in the central Indian Ocean, *Geology*, *37*, 455–458.

Konca, A. O., V. Hjorleifsdottir, T.-R. A. Song, J.-P. Avouac, D. V. Helmberger, C. Ji, K. Sieh, R. Briggs, and A. Meltzner (2007), Rupture kinematics of the 2005, Mw 8.6, Nias-Simeulue earthquake from the joint inversion of seismic and geodetic data, *Bull. Seismol. Soc. Am.*, *97*, S307–S322.

Le Dain, A. Y., P. Tapponnier, and P. Molnar (1984), Active faulting and tectonics of Burma and surrounding regions, *J. Geophys. Res.*, *89*, 453–472.

Lewis, S. E., R. A. J. Wust, J. M. Webster, and G. A. Shields (2008), Mid-late Holocene sea-level variability in eastern Australia, *Terra Nova*, *20*, 74–81.

Llovel, W., A. Cazenave, P. Rogel, and M. Berge-Nguyen (2009), 2-D reconstruction of past sea level (1950–2003) using tide gauge records and spatial patterns from a general ocean circulation model, *Clim. Past Discuss.*, *5*, 1109–1132.

Mallet, F. R. (1878), The Mud volcanoes of Ramri and Cheduba, *Geol. Surv. India Rec.*, *11*, part 2, 188–207.

Maurin, T., and C. Rangin (2009), Structure and kinematics of the Indo-Burmese Wedge: Recent and fast growth of the outer wedge, *Tectonics*, *28*, TC2010, doi:10.1029/2008TC002276.

Meltzner, A. J., K. Sieh, M. Abrams, D. C. Agnew, K. W. Hudnut, J.-P. Avouac, and D. H. Natawidjaja (2006), Uplift and subsidence associated with the great Aceh-Andaman earthquake of 2004, *J. Geophys. Res.*, *111*, B02407, doi:10.1029/2005JB003891.

Meltzner, A. J., K. Sieh, H.-W. Chiang, C.-C. Shen, B. W. Suwargadi, D. H. Natawidjaja, B. E. Philibosian, R. W. Briggs, and J. Galetzka (2010), Coral evidence for earthquake recurrence and an A.D. 1390–1455 cluster at the south end of the 2004 Aceh-Andaman rupture, *J. Geophys. Res.*, *115*, B10402, doi:10.1029/2010JB007499.

Natawidjaja, D. H., K. Sieh, J. Galetzka, B. W. Suwargadi, H. Cheng, R. L. Edwards, and M. Chlieh (2007), Interseismic deformation above the Sunda Megathrust recorded in coral microatolls of the Mentawai islands, West Sumatra, *J. Geophys. Res.*, *112*, B02404, doi:10.1029/2006JB004450.

Nielsen, C., N. Chamot-Rooke, C. Rangin, and The ANDAMAN Cruise Team (2004), From partial to full strain-partitioning along the Indo-Burmese hyper-oblique subduction, *Mar. Geol.*, *209*, 303-327.

Oldham, T. (1883), Catalogue of Indian Earthquakes, *Mem. Geol. Surv. India*, *19*(3), 170 pp.

Park, J. O., T. Tsuru, S. Kodaira, A. Nakanishi, S. Miura, Y. Kaneda, and Y. Kono (2000), Out-of-sequence thrust faults developed in the coseismic slip zone of the 1946 Nankai earthquake (Mw = 8.2) off Shikoku, southwest Japan, *Geophys. Res. Lett.*, *27*, 1033–1036.

Pirazzoli, P. A. (1986), Marine notches, in Sea-Level Research: A Manual for the Collection and Evaluation of Data, edited by O. V. van de Plassche, GeoBooks, Norwich.

Plafker, G. (1965), Tectonic deformation associated with the 1964 Alaska earthquake. *Science*, *148*, p. 1675–1687.

Plafker, G. (1972), Alaskan earthquake of 1964 and Chilean earthquake of 1960: Implications for arc tectonics, *J. Geophys. Res.*, *77*, 901–925.

Reimer, P. J., et al. (2009), IntCal09 and Marine09 radiocarbon age calibration curves, 0–50,000 years cal BP, *Radiocarbon*, *51*, 1111–1150.

Saillard, M., S. R. Hall, L. Audin, D. L. Farber, G. Hérail, J. Martinod, V. Regard, R. C. Finkel, and F. Bondoux (2009), Non-steady long-term uplift rates and Pleistocene marine terrace development along the Andean margin of Chile (31°S) inferred from ^{10}Be dating, *Earth Planet. Sci. Lett.*, *277*, 50–63.

Shen, C.-C., H. Cheng, R. L. Edwards, S. B. Moran, H. N. Edmonds, J. A. Hoff, and R. B. Thomas (2003), Measurement of attogram quantities of ^{231}Pa in dissolved and particulate fractions of seawater by isotope dilution thermal ionization mass spectroscopy, *Anal. Chem.*, *75*, 1075–1079.

Shen, C.-C., et al. (2012), High-precision and high-resolution carbonate ^{230}Th dating by MC-ICP-MS with SEM protocols, *Geochim. Cosmochim. Acta*, *99*, 71–86.

Shishikura, M., et al. (2009), Geomorphological evidence of great Holocene earthquakes of western Myanmar, *Proceedings of the International Workshop on Tsunami and Storm Surge Hazard Assessment and Management for Bangladesh*, CDMP, 35–40.

Socquet, A., C. Vigny, N. Chamot-Rooke, W. Simons, C. Rangin, and B. Ambrosius (2006), India and Sunda plates motion and deformation along their boundary in Myanmar determined by GPS, *J. Geophys. Res.*, *111*, B05406, doi:10.1029/2005JB003877.

Sugiyama, Y. (1994), Neotectonics of Southwest Japan due to the right-oblique subduction of the Philippine Sea Plate, *Geofisica Int.*, *33*, 53–76.

Taylor, F. W., R. W. Briggs, C. Frohlich, A. Brown, M. Hornbach, A. K. Papabatu, A. J. Meltzner, and D. Billy (2008), Rupture across arc segment and plate boundaries in the 1 April 2007 Solomons earthquake, *Nat. Geosci.*, *1*, 253–257.

ten Brink, U. S., J. Song, and R. C. Bucknam (2006), Rupture models for the A.D. 900–930 Seattle fault earthquake from uplifted shorelines, *Geology*, *34*, 585–588.

Than Tin Aung, K. Satake, Y. Okamura, M. Shishikura, Win Swe, Hla Saw, Tint Lwin Swe, Soe Thura Tun, and Thura Aung (2008), Geologic evidence for three great earthquakes in the past 3400 years off Myanmar, *J. Earthquake Tsunami*, *2*, 259–265.

Trenhaile A. S., and M. G. J. Layzell (1981), Shore platform morphology and the tidal duration factor, *Trans. Inst. Brit. Geogr., New Series*, *6*, 82–102.

U.S. Army Map Service (GDVLB) (1955a), Kyaukpyu, Burma, Sheet NE 46-3, Edition 1-AMS, 1:250,000, Series U542, U.S. Army, Washington, D. C.

U.S. Army Map Service (GDVLB) (1955b), Sandoway, Burma, Sheet NE 46-7, Edition 1-AMS, 1:250,000, Series U542, U.S. Army, Washington, D. C.

Wells, R. E., R. J. Blakely, Y. Sugiyama, D. W. Scholl, and P. A. Dinterman (2003), Basin-centered asperities in great subduction zone earthquakes: A link between slip, subsidence, and subduction erosion?, *J. Geophys. Res.*, *108*(B10), 2507, doi:10.1029/2002JB002072.

Woodroffe, S. A., and B. P. Horton (2005), Holocene sea level changes in the Indo-Pacific, *J. Asian Earth Sci.*, *25*, 29–43.

Xu, X., X. Wen, G. Yu, G. Chen, Y. Klinger, J. Hubbard, and J. Shaw (2009), Coseismic reverse- and oblique-slip surface faulting generated by the 2008 Mw7.9 Wenchuan earthquake, China, *Geology*, *37*, 515–518.

Zachariasen, J., K. Sieh, F. W. Taylor, R. L. Edwards, and W. S. Hantoro (1999), Submergence and uplift associated with the giant 1833 Sumatran subduction earthquake: Evidence from coral microatolls, *J. Geophys. Res.*, *104*, 895–919.

Zachariasen, J., K. Sieh, F. W. Taylor, and W. S. Hantoro (2000), Modern vertical deformation above the Sumatran subduction zone: Paleogeodetic insights from coral microatolls, *Bull. Seismol. Soc. Am.*, *90*, 897–913.